Structural Engineering and Mechanics, *Vol. 67, No. 5 (2018) 527-544*
DOI: https://doi.org/10.12989/sem.2018.67.5.527

Effect of homogenization models on stress analysis of functionally graded plates

Sihame Ait Yahia[1,2], Lemya Hanifi Hachemi Amar[3], Zakaria Belabed[2,4] and Abdelouahed Tounsi*[2,5]

[1]Département de Génie Civil, Faculté des Sciences Appliquées, Université Ibn Khaldoun, Tiaret, Algérie
[2]Material and Hydrology Laboratory, Faculty of Technology, Civil Engineering Department, University of Sidi Bel Abbes, Algeria
[3]Laboratoire des Ressources Hydriques et Environnement, Université Dr Tahar Moulay, BP 138 Cité En-Nasr 20000 Saida, Algérie
[4]Department of Technology, Institute of Science and Technology, Center University of Naama, Algeria
[5]Department of Civil and Environmental Engineering, King Fahd University of Petroleum & Minerals, 31261 Dhahran, Eastern Province, Saudi Arabia

(Received May 4, 2018, Revised June 6, 2018, Accepted June 7, 2018)

Abstract. In this paper, the effect of homogenization models on stress analysis is presented for functionally graded plates (FGMs). The derivation of the effective elastic proprieties of the FGMs, which are a combination of both ceramic and metallic phase materials, is of most of importance. The majority of studies in the last decade, the Voigt homogenization model explored to derive the effective elastic proprieties of FGMs at macroscopic-scale in order to study their mechanical responses. In this work, various homogenization models were used to derive the effective elastic proprieties of FGMs. The effect of these models on the stress analysis have also been presented and discussed through a comparative study. So as to show this effect, a refined plate theory is formulated and evaluated. , the number of unknowns and governing equations were reduced by dividing the transverse displacement into both bending and shear parts. Based on sinusoidal variation of displacement field trough the thickness, the shear stresses on top and bottom surfaces of plate were vanished and the shear correction factor was avoided. Governing equations of equilibrium were derived from the principle of virtual displacements. Analytical solutions of the stress analysis were obtained for simply supported FGM plates. The obtained results of the displacements and stresses were compared with those predicted by other plate theories available in the literature. This study demonstrates the sensitivity of the obtained results to different homogenization models and that the results generated may vary considerably from one theory to another. Finally, this study offers benchmark results for the multi-scale analysis of functionally graded plates.

Keywords: bending; stresses; FGM; plate theory; homogenization models

1. Introduction

In the last few decades, the evolution of the modern technology led several scientists to attempt to develop new materials with high performance characteristics. Functionally graded materials (FGMs) are considered as a relatively new class of composite materials, this class of materials has been found to be particularly useful in extremely high temperature environments which presented many advantages. In 1980's, a group of Japanese scientists proposed and designed FGMs to prepare thermal barrier materials (Yamanouchi *et al*. 1990, Koizumi 1993, 1997) for aerospace and aeronautical structures. A typical FGM is constituted of two distinct material phases (generally ceramic and metal or its alloy) , where the ceramic phase presents high thermal and corrosion resistances and the metallic phase presents high strength and better toughness, the mechanical properties of FGM change continuously and smoothly through the thickness coordinate. These characteristics eliminate and reduce the influence of stress concentration unlike laminated composites, this combination produces new materials with superior properties, and these advantages have accelerated the implementation of functionally graded materials in diverse engineering applications (Behravan Rad 2012, Sobhy 2013; Hebali *et al.* 2014, Bousahla *et al.* 2014, Bourada *et al*. 2015, Larbi Chaht *et al*. 2015, Kar and Panda 2015, Hamidi *et al.* 2015, Bounouara *et al.* 2016, Abdelaziz *et al*. 2017, Khetir *et al.* 2017, Benadouda *et al*. 2017, Bouafia *et al*. 2017, Chikh *et al.* 2017, Sekkal *et al.* 2017a, b, El-Haina *et al.* 2017, Shahsavari *et al.* 2018, Bakhadda *et al.* 2018, Fourn *et al.* 2018, Abualnour *et al.* 2018, Bouhadra *et al.* 2018, Karami *et al.* 2018a, b, c). The FGM structures have been gaining wide use in different fields but the most important factor is to have comprehension of their mechanical behaviors relative to the properties of ceramic and metal material phases at the macroscopic level.

Homogenization procedures consist to transform a composite medium to an equivalent homogeneous medium at macroscopic scale; the aim of these procedures is to predict correctly the effective properties of composites such as functionally graded materials. To know the basic concept of FGMs, it is very necessary to collect all information about their constituents, such as the interfaces between

*Corresponding author, Professor
E-mail: tou_abdel@yahoo.com

http://www.techno-press.com/journals/sem&subpage=7 ISSN: 1225-4568 (Print), 1598-6217 (Online)

matrix and inclusions, and their geometry, arrangement and volume fraction. Moreover, the homogenization procedures are based on two essential steps; the first one consist of the experimental measurements of FGM constituents and the extraction of their physical properties, and the second one is the estimation of the effective proprieties using the correct method according to the interaction of the inclusions with the matrix. Analysis of the literature dealing with homogenization of functionally graded materials can be carried on several homogenization models, thus models have been conveniently grouped into two basic classifications: analytical and numerical models. Analytical models are widely used to derive the effective elastic proprieties of functionally graded materials. However, various homogenization models have been detailed and discussed to estimate the effective properties of functionally graded materials, based on volume fraction distribution by Zuiker (1995) who elaborated the importance of limitation on structural mechanics property variation. Gasik (1998) presented many homogenization models used for composites and functionally graded materials and discussed the effect of the derived effective thermo-mechanical properties of these models on elastic and plastic thermal stress analysis of FGMs. Paulino *et al.* (2003) elucidated on a range of micro-mechanics models for predicting the elastic effective proprieties of FGMs and their failure behavior. Yin *et al.* (2004) obtained novel results via a micromechanical model for the effective elastic behavior of functionally graded materials with particle interactions based on Eshelby's equivalent inclusion method. Yin *et al.* (2007) discussed micromechanics solutions based on a thermoelastic model for the effective coefficient of thermal expansion in a detailed simulation of thermomechanical behavior of FGMs. Rahman and Chakraborty (2007) presented a stochastic micromechanical model to derive the effective proprieties of functionally graded materials including the statistical uncertainties in material properties of material constituents, particle and porosity and their respective volume fractions. Birman and Byrd (2007) provided a general and extensive review on homogenization models of the property distribution applicable to functionally graded materials. Klusemann and Svendsen (2010) reviewed and compared various classical homogenization models to derive the elastic properties and their behaviors for general two-phase composite materials.

On the other hand, the improvement of numerical simulations has led to brought important enhancements in predicting the effective proprieties of FGMs , Reiter and Dvorak (1997) presented a numerical simulation based on Mori-Tanaka method to predict the elastic responses for several functionally graded microstructures under different traction and mixed boundary conditions. An extension of this work for thermomechanical loading was subsequently communicated by Reiter and Dvorak (1998). Cho and Ha (2001) compared results obtained by two classical averaging approaches for predicting the Young's modulus and the thermal expansion coefficient for functionally graded materials, namely the Wakashima-Tsukamoto linear modified mixture rule and the finite-element discretization approach utilizing rectangular cells. Schmauder and Weber (2001) presented numerical results for homogenization modeling of functionally graded materials also benchmarking their solutions with experimental findings. Shabana and Noda (2008) employed a homogenization model and finite element approach to derive the effective thermo-mechanical proprieties for the transient thermal conduction problem.

This short review on homogenization models applied to determine the effective physical proprieties of FGMs is limited to micro-scale of these materials; the transition from micro-scale to macro-scale is more needed to solve engineering problems. The mechanical behavior of functionally graded plates has been widely investigated by many researchers in recent years. In most of investigations, the Voigt model was extensively adopted to determine the effective physical properties for macro-responses of functionally graded plates. Nevertheless, it is observed that in many research papers dealing with functionally graded plates, the effect of homogenization models is relatively neglected and their impact on mechanical behaviors of FGM plates is discussed only by particular studies.

The mathematical modeling of FGM plates presents a practical procedure to evaluate the material properties based on appropriate homogenization model. Several comprehensive studies are available for providing a good methodology with regard to predicting the effect of homogenization models on functionally graded plate behaviors at the macroscopic scale. Vel and Batra (2004) used the Mori-Tanaka and self-consistent schemes to obtain three-dimensional exact solutions for vibration response of functionally graded rectangular plates, although they did not deliberate to any great extent on the physical implications of their solutions. Ferreira *et al.* (2005) estimated the effective proprieties by the rule of mixtures and the Mori-Tanaka scheme to analyze static deformations of a simply supported functionally graded plate. Ferreira et al. (2006) later presented solutions for the free vibration of functionally graded plates based on third-order shear deformation plate theories. Shen *et al.* (2012) assessed the viability of both the Voigt and Mori-Tanaka models for vibration analysis of functionally graded plates. Belabed *et al.* (2014) presented an efficient and simple higher order shear plate theory, considering three distribution material models (i.e., the power law distribution, the exponential distribution, and the Mori-Tanaka scheme) to derive elastic proprieties for both static and dynamic cases. Akbarzadeh *et al.* (2015) explored the relative performance of a diverse range of homogenization models (i.e., Voigt, Reuss, Hashin-Shtrikman bounds, LRVE and self-consistent models)and their effect on the static and dynamic stress fields, critical buckling loads, and fundamental frequency of functionally graded plate resting on a Pasternak elastic foundation. Akavci *et al.* (2015) adopted the Mori-Tanaka, power-law and exponential distributions models to estimate the effective properties of graded materials with new higher order shear deformation theories for static and free vibration analysis. Thai *et al.* (2016) considered two homogenization models (i.e., the mixture rule and the Mori-Tanaka method) for deriving closed-form solutions for static, dynamic and buckling behavior of isotropic functionally graded material sandwich plates. Tossapanon and Wattanasakulpong (2016) compared the buckling and free vibration of functionally graded sandwich beams resting on a two-parameter elastic foundation based on the rules of mixture and the Mori–Tanaka method. Gupta and Talha (2016) used the Voigt model and Mori-Tanaka method to predict the effective properties of vibration response of functionally graded plates with initial geometric imperfections. Su *et al.* (2016) discussed the effect of homogenization models based on Voigt and Mori-Tanaka approaches on free vibration of functionally graded sandwich beams with general boundary conditions and resting on a Pasternak elastic foundation. Liu *et al.* (2016) presented a comparative study based on Voigt's rule and Mori-Tanaka scheme to investigate the free vibration response of functionally graded sandwich and laminated shells. Farzam-Rad *et al.* (2017) employed the rule of mixtures and Mori-Tanaka scheme for the static and free vibration analysis of functionally graded and sandwich plates. Recently, Aldousari (2017) studied the bending behavior of rectangular functionally graded beams subjected to transverse loading with different material distributions and a Galerkin finite element formulation.

The increasing use of functionally graded plates requires an efficient and simple plate theory to predict correctly the mechanical behavior of such structural elements. Many studies have been presented on accurate plate theories to simulate static, buckling and dynamic behaviors of functionally graded plates. Founded on the kinematic field assumptions, these plate theories are developed in accordance with the plate thickness-to-length ratio. To achieve improved accuracy, various higher-order shear deformation plate theories (HSDTs) have been developed and implemented in recent years to analyze the responses of thick functionally graded plates in various loading scenarios. These theories are capable of much better representation of the distribution of displacement, strains and stresses through the thickness of plate compared with classical plate theory and First-order shear deformation theory. However, the resulting equations of motion are much more complicated since they invariably generate a host of unknowns. Recently, an accurate refined higher order shear deformation theory (RHSDT) has been developed which is relatively simple to use and simultaneously retains important physical characteristics. The use of refined plate theories overcomes the limits of classical, first order and higher order plate theories. In fact, the application of the RHSDT formulation (with only four or two unknowns) to various problems (e.g., bending, buckling , thermal and dynamics) of FGM plates is advised in Bouderba *et al.*(2013), Bachir Bouiadjra *et al.* (2013), Ait Amar *et al.* (2014), Zidi *et al.*(2014), Ait Yahia *et al.*(2015), Attia *et al.* (2015), Bakora *et al.*(2015), Bouderba *et al.* (2016), Boukhari *et al.* (2016), Barati *et al.* (2016), Beldjelili *et al.* (2016), Karami and Janghorban (2016), Bousahla *et al.* (2016), Karami *et al.* (2017a), Shahsavari and Janghorban (2017), Fahsi *et al.* (2017), Younsi *et al.* (2018), Meksi *et al.* (2018) and Benchohra *et al.* (2018). The displacement field is chosen based on a nonlinear variation of in-plane and transverse displacements through the thickness. Partitioning the transverse displacement into the bending and shear components leads to a reduction in the number of unknowns, and consequently, makes these theories much more amenable to mathematical implementation. Recently, the refined higher-order plate theories (Polynomial, Exponential, and Hyperbolic) needless of any shear correction factor are used by Shahsavari *et al.* (2018). Shear deformation theories are also applied to investigate the mechanical behavior of nanocomposite structures (Kolahchi and Moniri Bidgoli 2016, Madani *et al.* 2016, Kolahchi *et al.* 2016a, b, Arani and Kolahchi 2016, Bilouei *et al.* 2016, Kolahchi *et al.* 2017a, b, c, Kolahchi and Cheraghbak 2017, Kolahchi *et al.* 2017a, Zamanian *et al.* 2017, Kolahchi 2017, Shokravi 2017a, b, c, d, Hajmohammad *et al.* 2017, 2018a, b, c, Zarei *et al.* 2017, Amnieh *et al.* 2018, Golabchi *et al.* 2018).

In this study, the effect of homogenization models on stress analysis is investigated for thick functionally graded plates. To evaluate the effective elastic proprieties such as Young's modules and Poisson's ratio, a range of explicit homogenization models are utilized such as the Voigt, Reuss, Hashin-Shtrikman bounds Tamura and LRVE models based on volume fraction distribution. It should be noted that the effect of the micromechanical models is recently studied by Bachir Bouiadjra *et al.* (2018) with considering the stretching effect. However, in this paper other micromechanical models are employed such as Hashin-Shtrikman bounds model to explain in a rigorous way this effect. As to the plate analysis, the refined plate theory for functionally graded plates is proposed to predict the bending and stresses of thick FGM plates. These theories delineates the transverse displacement into both bending and shear parts with only four-unknowns, and therefore decreases the number of governing equations. A sinusoidal variation is elected for all displacements across the thickness which satisfies the stress-free boundary conditions on the upper and lower surfaces of the plate without requiring any shear correction factor. The governing equilibrium equations and boundary conditions are derived from principle of virtual displacements. Analytical solutions for bending and stresses are obtained. Numerical examples are presented and compared with those obtained by classical and third-order plate theories using different homogenization models showing significant difference in results. Finally, the present study, which is generally neglected in the vast majority of investigations, shows that structural responses of functionally graded plates can be correctly evaluated by the correct choice of the constituent materials and their homogenization models.

2. Homogenization models for functionally graded materials

The homogenization model deals with the mechanical behaviors of FGM plates as it considers the interaction of the inclusions with the matrix, the material properties of FGM plates are assumed to change continuously through the plate thickness based on the volume fraction of inclusions. The power-law distribution is introduced for the distribution of volume fraction of FGM constituents as follows (Zenkour 2006, Attia *et al.* 2015, 2018, Mahi *et al.* 2015, Mouffoki *et al.* 2017, Zidi *et al.* 2017, Belabed *et al.* 2018)

$$V_f(z) = V_m + (V_c - V_m)\left(\frac{2z+h}{2h}\right)^p \tag{1}$$

Where p is the power law material index parameter and the subscripts m and c represent the metallic and ceramic phases, respectively. The homogenization models are deployable for the computation of the Young's modulus $E(z)$ and Poisson's ratio $\upsilon(z)$, thus models are setting up under basic assumptions, such as the interface of the constituents is bonded continuously from a ceramic-rich surface to a metal-rich surface according to selected volume fraction distributions, each constituent is considered macroscopically homogenous, linearly elastic and isotropic, no porosities were included in FGM and the linear elasticity and initially stress-free assumptions are adopted . In this study, the FGM properties are derived via explicit homogenization models such as Voigt, Reuss, Hashin-Shtrikman bounds, Tamura and Cubic local representative volume elements (LRVE) models which can be described as follows.

2.1 Voigt model

Voigt or rule of mixture model presents the well-known models of homogenization used to derive the effective elastic properties for various class of composite materials, it has been initially proposed by Voigt (1889), the basic idea of this model is to estimate the effective proprieties of FGM by considering the equivalent strain energy approach that the strain induced is considered constant through the material coordinate loading, for both matrix and inclusions elementary volumes. Appling the assumption of Voigt for functionally graded materials, the Young's modulus is given as (Bellifa *et al.* 2016)

$$E(z) = E_c V_f(z) + E_m(1 - V_f(z)) \tag{2}$$

and the related Poisson's ratio is assumed as

$$\upsilon(z) = \upsilon_c V_f(z) + \upsilon_m(1 - V_f(z)) \tag{3}$$

2.2 Reuss model

Reuss (1929) has derived expressions for the effective proprieties of anisotropic materials consisting of homogeneous phases, the assumption of total average stress at macroscopic scale is considered identical in each phase under equivalent uniform stress, and this model is also known as inverse rule of Voigt model. This model produces estimation of the Young's modulus and Poisson's ratio respectively as

$$E(z) = \frac{E_c E_m}{E_c(1 - V_f(z)) + E_m V_f(z)} \tag{4}$$

and,

$$\upsilon(z) = \frac{\upsilon_c \upsilon_m}{\upsilon_c(1 - V_f(z)) + \upsilon_m V_f(z)} \tag{5}$$

Hill (1963) much later showed that the Voigt and Reuss rules present the upper and lower bounds respectively of the elastic effective proprieties of reinforced solids and their assumptions can been derived from the energy principles, as defined by Hill's condition (Hazanov 1998).

2.3 Hashin-Shtrikman bounds model

Hashin and Shtrikman (1963) proposed expressions to derive the effective elastic proprieties provided the lower and upper bounds for two-phase materials, the presented assumption was based on variational energy principles of both strain and stress fields. As a result, the effective proprieties were given as a function of the bulk (K (z) and shear modulus (G (z), The Young's modulus can be stated in the form

$$E(z) = \frac{9G(z)K(z)}{G(z) + 3K(z)} \tag{6}$$

Poisson's ratio is given as

$$\upsilon(z) = \frac{3K(z) - 2G(z)}{2G(z) + 6K(z)} \tag{7}$$

where $G(z)$ and $K(z)$ denote the shear and bulk modulus through the thickness respectively;

$$\left.\begin{aligned} G^{Low}(z) &= G_m + \cfrac{V_f(z)}{\cfrac{1}{G_c - G_m} + \cfrac{6(K_m + 2G_m)(1 - V_f(z))}{5G_m(3K_m + 4G_m)}} \\ K^{Low}(z) &= K_m + \cfrac{V_f(z)}{\cfrac{1}{K_c - K_m} + \cfrac{3(1 - V_f(z))}{(3K_m + 4G_m)}} \end{aligned}\right\} \tag{8}$$

for lower bound
and,

$$\left.\begin{aligned} G^{Up}(z) &= G_c + \cfrac{V_f(z)}{\cfrac{1}{G_m - G_c} + \cfrac{6(K_c + 2G_c)(1 - V_f(z))}{5G_c(3K_c + 4G_c)}} \\ K^{Up}(z) &= K_c + \cfrac{V_f(z)}{\cfrac{1}{K_m - K_c} + \cfrac{3(1 - V_f(z))}{(3K_c + 4G_c)}} \end{aligned}\right\} \tag{9}$$

for upper bound

In fact, the upper and lower bounds describe the contrast in material properties or phases of the matrix and inclusions.

2.4 Tamura model

This model is based on the empirical fitting parameter q_T called the "stress-to-strain transfer" (Zuiker 1995, Gasik 1998) which is derived from coupling the stress and strain averages under uniaxial uniform loading of two phase materials such as ceramic and metal materials, defined us

$$q_T = \frac{(\sigma_c - \sigma_m)}{E_c(\varepsilon_c - \varepsilon_m)} \tag{10}$$

The emerging effective Young's modulus for this model described below

$$E(z) = \frac{(1-V_f(z))E_m(q_T - E_c) + V_f(z)E_c(q_T - E_m)}{(1-V_f(z))(q_T - E_c) + V_f(z)(q_T - E_m)} \tag{11}$$

It is clearly that for q_T=0, Reuss's model is retrieved as a special case. Furthermore Voigt's model corresponds to the case given by $q_T=\pm\infty$. Poisson's ratio is derived from Voigt's model as

$$\upsilon(z) = \upsilon_c V_f(z) + \upsilon_m(1 - V_f(z)) \tag{12}$$

2.5 Cubic local representative volume elements (LRVE) model

Gasik and Lilius (1994) formulated a new micro-mechanical model to predict the effective elastic proprieties which can be obtained by spatial translations of a repetitive volume element or elementary unit cell. This intermediate scale is termed the cubic local representative volume element (LRVE) which relates the strain and stress components on the local representative element surfaces at the infinite length scale. These assumptions are applied to Young's modulus as follows

$$E(z) = E_m\left(1 - \sqrt[3]{V_f(z)}\left(1 - \frac{1}{1 - \sqrt[3]{V_f(z)}\left(1 - E_m/E_c\right)}\right)\right) \tag{13}$$

By simplification, the Young's modulus is easily obtained as

$$E(z) = E_m\left(1 + \frac{V_f(z)}{FE - \sqrt[3]{V_f(z)}}\right) \tag{14}$$

Wherein

$$FE = \frac{1}{1 - E_m/E_c} \tag{15}$$

Additionally, Poisson's ratio emerges in the same form as for the Voigt model

$$\upsilon(z) = \upsilon_c V_f(z) + \upsilon_m(1 - V_f(z)) \tag{16}$$

The variation of the effective Young's modulus of used homogenization models is shown in Fig. 1 with the material index parameter is taken p=1. It is clearly visible that the used homogenization models result in different estimations for the same homogenized Young's modulus, this distinction is accorded to the basic assumptions of each homogenization model. Voigt's model achieves the maximum of averaging Young's modulus based on lower

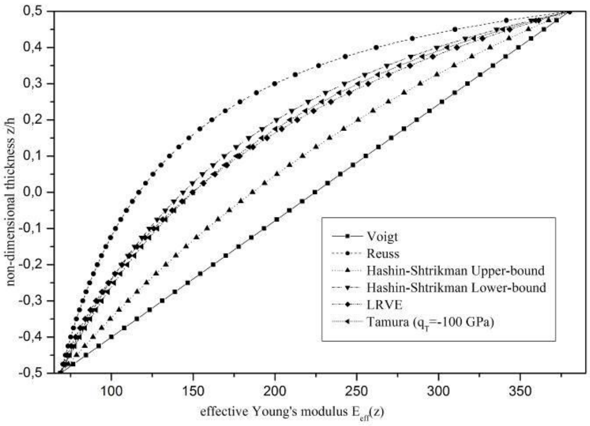

Fig. 1 The effective Young's modulus of Al/Al_2O_3 FGM plate using different homogenization models (p=1)

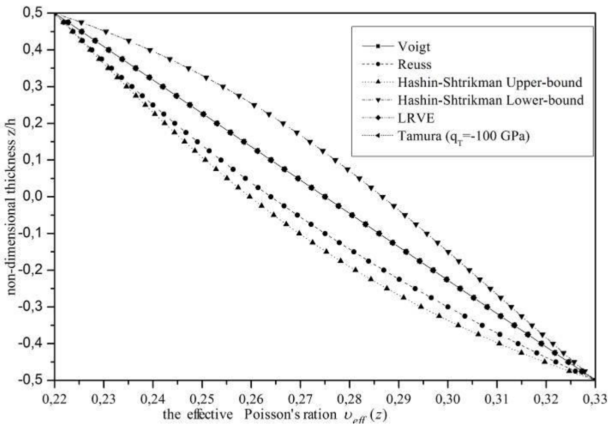

Fig. 2 The effective Poisson's ratio of Al/Al_2O_3 FGM plate using different homogenization models (p=1)

bound estimates of the ceramic phase material. The minimum value of Young's modulus corresponds to the Reuss model which considers the upper bound in which presents the metallic material phase to determine this physical parameter. It is observed that the Hashin-Shtrikman (Lower Bound), Tamura and LRVE models predict similar values of Young's modulus compared to other used models. Most of the earliest FGM studies are based on Voigt's model to predict the effective Young's modulus, but there are many considerations taken into account to evaluate correctly this physical parameter such as the geometry of inclusions, their arrangement and interaction with the matrix. Moreover, this difference in presented values of Young's modulus leads to an important impact on mechanical behaviors of FGM plates at macro-scale, which will be discussed in this proposed study. For simplicity, many researchers had considered Poisson's ratio to be constant, the variation presented in Fig. 2 for Poisson's ratio demonstrates that it is necessary to take in account this variation in mechanical computations to predict correctly FGM plate mechanical responses. It should be noted that Voigt, Tamura and LRVE models use the same law to derive the effective Poisson's ratio. Also the Reuss and Hashin- Shtrikman (L.B) models assumed the effective Poisson's ratio by introduction the physical characteristics of the lower bound (L.B) which under-predict this physical parameter compared to other models. Hashin-Shtrikman (U.B) model estimates the effective Poisson's ratio based on the upper bound which yields the maximum values of this physical parameter. For material index parameter p=1, Voigt's model presents a linear variation of Poisson's ratio through the thickness. This simple variation is given as function of the FGM Poisson's ratio from fully ceramic to fully metallic bounds.

3. Theoretical formulation

3.1 Kinematics

The displacement field of the present theory is chosen based on the following assumptions: (1) The transverse displacements are partitioned into bending and shear components; (2) the in-plane displacement is partitioned into extension, bending and shear components; (3) the bending parts of the in-plane displacements are similar to those given by CPT ; and (4) the shear parts of the in-plane displacements give rise to the sinusoidal variations of shear strains and hence to shear stresses through the thickness of the plate in such a way that the shear stresses vanish on the top and bottom surfaces of the plate. Based on these assumptions, the following displacement field relations can be obtained (Tounsi *et al.* 2013, Zemri *et al.* 2015, Attia *et al.* 2015, Ait Yahia *et al.* 2015, Belkorissat *et al.* 2015, Bennoun *et al.* 2016)

$$u(x,y,z)=u_0(x,y)-z\frac{\partial w_b}{\partial x}-f(z)\frac{\partial w_s}{\partial x} \tag{17a}$$

$$v(x,y,z)=v_0(x,y)-z\frac{\partial w_b}{\partial y}-f(z)\frac{\partial w_s}{\partial y} \tag{17b}$$

$$w(x,y,z)=w_b(x,y)+w_s(x,y) \tag{17c}$$

where u_0 and v_0 denote the displacements along the x and y coordinate directions of a point on the mid-plane of the plate; w_b and w_s are the bending and shear components of the transverse displacement, respectively. In this study, the shape function $f(z)$ is chosen based on the sinusoidal function proposed by Touratier (1991) as

$$f(z)=z-\frac{h}{\pi}\sin\left(\frac{\pi z}{h}\right) \tag{18}$$

The non-zero strains associated with the displacement field in Eq. (16) are

$$\begin{Bmatrix}\varepsilon_x\\ \varepsilon_y\\ \gamma_{xy}\end{Bmatrix}=\begin{Bmatrix}\varepsilon_x^0\\ \varepsilon_y^0\\ \gamma_{xy}^0\end{Bmatrix}+z\begin{Bmatrix}k_x^b\\ k_y^b\\ k_{xy}^b\end{Bmatrix}+f(z)\begin{Bmatrix}k_x^s\\ k_y^s\\ k_{xy}^s\end{Bmatrix} \tag{19a}$$

$$\begin{Bmatrix}\gamma_{yz}\\ \gamma_{xz}\end{Bmatrix}=g(z)\begin{Bmatrix}\gamma_{yz}^0\\ \gamma_{xz}^0\end{Bmatrix}, \tag{19b}$$

where

$$\begin{Bmatrix}\varepsilon_x^0\\ \varepsilon_y^0\\ \gamma_{xy}^0\end{Bmatrix}=\begin{Bmatrix}\dfrac{\partial u_0}{\partial x}\\ \dfrac{\partial v_0}{\partial x}\\ \dfrac{\partial u_0}{\partial y}+\dfrac{\partial v_0}{\partial x}\end{Bmatrix},\quad \begin{Bmatrix}k_x^b\\ k_y^b\\ k_{xy}^b\end{Bmatrix}=\begin{Bmatrix}-\dfrac{\partial^2 w_b}{\partial x^2}\\ -\dfrac{\partial^2 w_b}{\partial y^2}\\ -2\dfrac{\partial^2 w_b}{\partial x\partial y}\end{Bmatrix},$$

$$\begin{Bmatrix}k_x^s\\ k_y^s\\ k_{xy}^s\end{Bmatrix}=\begin{Bmatrix}-\dfrac{\partial^2 w_s}{\partial x^2}\\ -\dfrac{\partial^2 w_s}{\partial y^2}\\ -2\dfrac{\partial^2 w_s}{\partial x\partial y}\end{Bmatrix}, \tag{20a}$$

$$\begin{Bmatrix}\gamma_{yz}^0\\ \gamma_{xz}^0\end{Bmatrix}=\begin{Bmatrix}\dfrac{\partial w_s}{\partial y}\\ \dfrac{\partial w_s}{\partial x}\end{Bmatrix}, \tag{20b}$$

and

$$g(z)=1-\frac{df(z)}{dz} \tag{21}$$

3.2 Equilibrium equations

The principle of virtual displacements is used herein to derive the governing equations for FGM plates, this principle can be stated in an analytical form as follows (Ait Atmane *et al.* 2015, Al-Basyouni *et al.* 2015, Meradjah *et al.*2015, Draiche *et al.* 2016, Ahouel *et al.* 2016, Houari *et al.* 2016, Bellifa *et al.* 2017a, b, Besseghier *et al.* 2017, Klouche *et al.* 2017, Hachemi *et al.* 2017, Menasria *et al.* 2017, Yazid *et al.* 2018, Kaci *et al.* 2018, Zine *et al.* 2018, Mokhtar *et al*. 2018, Youcef *et al.* 2018)

$$\int_{-h/2}^{h/2}\int_A(\delta U+\delta V)dA dz=0 \tag{22}$$

where δU is the variation of strain energy and δV is the variation of potential energy. The variation of strain energy of the plate is calculated by

$$\begin{aligned}\delta U&=\int_{-h/2}^{h/2}\int_A\left[\sigma_x\delta\varepsilon_x+\sigma_y\delta\varepsilon_y+\tau_{xy}\delta\gamma_{xy}+\tau_{yz}\delta\gamma_{yz}+\tau_{xz}\delta\gamma_{xz}\right]dA\,dz\\&=\int_A\left[N_x\delta\varepsilon_x^0+N_y\delta\varepsilon_y^0+N_{xy}\delta\gamma_{xy}^0+M_x^b\delta k_x^b+M_y^b\delta k_y^b+M_{xy}^b\delta k_{xy}^b\right.\\&\quad\left.+M_x^s\delta k_x^s+M_y^s\delta k_y^s+M_{xy}^s\delta k_{xy}^s+S_{yz}^s\delta\gamma_{yz}^0+S_{xz}^s\delta\gamma_{xz}^0\right]dA=0\end{aligned} \tag{23}$$

where A is the top surface and the stress resultants N, M and S are defined by

$$\begin{Bmatrix}N_x,\ N_y,\ N_{xy}\\ M_x^b,M_y^b,M_{xy}^b\\ M_x^s,M_y^s,M_{xy}^s\end{Bmatrix}=\int_{-h/2}^{h/2}(\sigma_x,\sigma_y,\tau_{xy})\begin{Bmatrix}1\\ z\\ f(z)\end{Bmatrix}dz, \tag{24a}$$

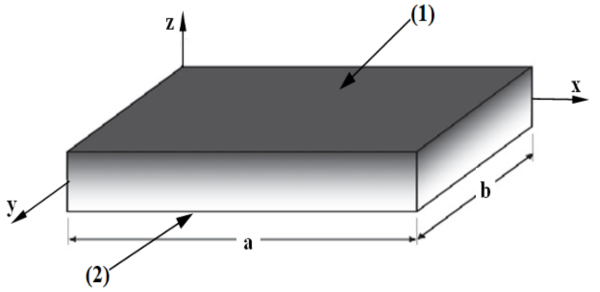

Fig. 3 FGM plate (1) metal-rich surface (2) ceramic-rich surface

$$\left(S_{xz}^{s}, S_{yz}^{s}\right) = \int_{-h/2}^{h/2} \left(\tau_{xz}, \tau_{yz}\right) g(z) dz. \tag{24b}$$

The variation of potential energy of the external applied loads can be expressed thus

$$\delta V = -\int_{A} q \delta \left(w_b + w_s\right) dA \tag{25}$$

where q is the distributed transverse load.

Substituting the expressions for δu and δV from Eqs. (23) and (25) into Eq. (22) and integrating by parts, and collecting the coefficients of δu_0, δv_0, δw_b and $\overline{w}$, the following equations of the plate are obtained

$$\delta u_0 : \frac{\partial N_x}{\partial x} + \frac{\partial N_{xy}}{\partial y} = 0 \tag{26a}$$

$$\delta v_0 : \frac{\partial N_{xy}}{\partial x} + \frac{\partial N_y}{\partial y} = 0 \tag{26b}$$

$$\delta w_b : \frac{\partial^2 M_x^b}{\partial x^2} + 2\frac{\partial^2 M_{xy}^b}{\partial x \partial y} + \frac{\partial^2 M_y^b}{\partial y^2} - q = 0 \tag{26c}$$

$$\delta w_s : \frac{\partial^2 M_x^s}{\partial x^2} + 2\frac{\partial^2 M_{xy}^s}{\partial x \partial y} + \frac{\partial^2 M_y^s}{\partial y^2} + \frac{\partial S_{xz}^s}{\partial x} + \frac{\partial S_{yz}^s}{\partial y} - q = 0 \tag{26d}$$

The natural boundary conditions are of the form

$$\delta u_0 : N_x n_x + N_{xy} n_y \tag{27a}$$

$$\delta v_0 : N_{xy} n_x + N_y n_y \tag{27b}$$

$$\delta w_b : \left(\frac{\partial M_x^b}{\partial x} + \frac{\partial M_{xy}^b}{\partial y}\right) n_x + \left(\frac{\partial M_{xy}^b}{\partial x} + \frac{\partial M_y^b}{\partial y}\right) n_y + \frac{\partial M_{ns}^b}{\partial s} \tag{27c}$$

$$\delta w_s : \left(S_{xz}^s + \frac{\partial M_x^s}{\partial x} + \frac{\partial M_{xy}^s}{\partial y}\right) n_x + \left(S_{yz}^s + \frac{\partial M_{xy}^s}{\partial x} + \frac{\partial M_y^s}{\partial y}\right) n_y + \frac{\partial M_{ns}^s}{\partial s} \tag{27d}$$

$$\frac{\partial \delta w_b}{\partial n} : M_n^b \tag{27e}$$

$$\frac{\partial \delta w_s}{\partial n} : M_n^s \tag{27f}$$

where

$$\begin{gathered} M_{ns}^b = \left(M_y^b - M_x^b\right) n_x n_y + M_{xy}^b \left(n_x^2 - n_y^2\right), \\ M_n^b = M_x^b n_x^2 + M_y^b n_y^2 + 2 M_{xy}^b n_x n_y \end{gathered} \tag{28a}$$

$$\begin{gathered} M_{ns}^s = \left(M_y^s - M_x^s\right) n_x n_y + M_{xy}^s \left(n_x^2 - n_y^2\right), \\ M_n^s = M_x^s n_x^2 + M_y^s n_y^2 + 2 M_{xy}^s n_x n_y \end{gathered} \tag{28b}$$

$$\frac{\partial}{\partial n} = n_x \frac{\partial}{\partial x} + n_y \frac{\partial}{\partial y}, \quad \frac{\partial}{\partial s} = n_x \frac{\partial}{\partial x} - n_y \frac{\partial}{\partial y} \tag{28c}$$

3.3 Constitutive equations

The linear constitutive relations of a FGM plate can be written as

$$\begin{Bmatrix} \sigma_x \\ \sigma_y \\ \tau_{yz} \\ \tau_{xz} \\ \tau_{xy} \end{Bmatrix} = \begin{bmatrix} C_{11} & C_{12} & 0 & 0 & 0 \\ C_{12} & C_{22} & 0 & 0 & 0 \\ 0 & 0 & C_{44} & 0 & 0 \\ 0 & 0 & 0 & C_{55} & 0 \\ 0 & 0 & 0 & 0 & C_{66} \end{bmatrix} \begin{Bmatrix} \varepsilon_x \\ \varepsilon_y \\ \gamma_{yz} \\ \gamma_{xz} \\ \gamma_{xy} \end{Bmatrix} \tag{29}$$

where (σ_x, σ_y, τ_{yz}, τ_{xz}, τ_{xy}) and (ε_x, ε_y, γ_{yz}, γ_{xz}, γ_{xy}) are the stress and strain components, respectively.

The elastic constants C_{ij} are the plane stress reduced elastic constants, defined as

$$C_{11} = C_{22} = \frac{E(z)}{1 - \nu(z)^2}, \quad C_{12} = \nu(z) C_{11}, \tag{30a}$$

$$C_{44} = C_{55} = C_{66} = G(z) = \frac{E(z)}{2\left(1 + \nu(z)\right)}. \tag{30b}$$

E, G and the elastic coefficients C_{ij} vary through the thickness according to Eqs. (2), (4), (6), (11) or (14). By substituting Eq. (19) into Eq. (29) and the subsequent results into Eq. (24), the stress resultants are readily obtained as

$$\begin{Bmatrix} N \\ M^b \\ M^s \end{Bmatrix} = \begin{bmatrix} A & B & B^s \\ B & D & D^s \\ B^s & D^s & H^s \end{bmatrix} \begin{Bmatrix} \varepsilon \\ k^b \\ k^s \end{Bmatrix}, \tag{31a}$$

$$S = A^s \gamma \tag{31b}$$

where

$$\begin{gathered} N = \left\{N_x, N_y, N_{xy}\right\}, \quad M^b = \left\{M_x^b, M_y^b, M_{xy}^b\right\}, \\ M^s = \left\{M_x^s, M_y^s, M_{xy}^s\right\}, \end{gathered} \tag{32a}$$

$$\begin{gathered} \varepsilon = \left\{\varepsilon_x^0, \varepsilon_y^0, \gamma_{xy}^0\right\}, \quad k^b = \left\{k_x^b, k_y^b, k_{xy}^b\right\}, \\ k^s = \left\{k_x^s, k_y^s, k_{xy}^s\right\}, \end{gathered} \tag{32b}$$

$$\begin{gathered} A = \begin{bmatrix} A_{11} & A_{12} & 0 \\ A_{12} & A_{22} & 0 \\ 0 & 0 & A_{66} \end{bmatrix}, \quad B = \begin{bmatrix} B_{11} & B_{12} & 0 \\ B_{12} & B_{22} & 0 \\ 0 & 0 & B_{66} \end{bmatrix}, \\ D = \begin{bmatrix} D_{11} & D_{12} & 0 \\ D_{12} & D_{22} & 0 \\ 0 & 0 & D_{66} \end{bmatrix}, \end{gathered} \tag{32c}$$

$$B^s = \begin{bmatrix} B_{11}^s & B_{12}^s & 0 \\ B_{12}^s & B_{22}^s & 0 \\ 0 & 0 & B_{66}^s \end{bmatrix}, \quad D^s = \begin{bmatrix} D_{11}^s & D_{12}^s & 0 \\ D_{12}^s & D_{22}^s & 0 \\ 0 & 0 & D_{66}^s \end{bmatrix}, \quad H^s = \begin{bmatrix} H_{11}^s & H_{12}^s & 0 \\ H_{12}^s & H_{22}^s & 0 \\ 0 & 0 & H_{66}^s \end{bmatrix}, \tag{32d}$$

$$S = \{S_{xz}^s, S_{yz}^s\}, \quad \gamma = \{\gamma_{xz}, \gamma_{yz}\}, \quad A^s = \begin{bmatrix} A_{44}^s & 0 \\ 0 & A_{55}^s \end{bmatrix}, \tag{32e}$$

Here the stiffness coefficients are defined as

$$\begin{Bmatrix} A_{11} & B_{11} & D_{11} & B_{11}^s & D_{11}^s & H_{11}^s \\ A_{12} & B_{12} & D_{12} & B_{12}^s & D_{12}^s & H_{12}^s \\ A_{66} & B_{66} & D_{66} & B_{66}^s & D_{66}^s & H_{66}^s \end{Bmatrix} = \int_{-h/2}^{h/2} C_{11}\left(1, z, z^2, f(z), z\, f(z), f^2(z)\right) \begin{Bmatrix} 1 \\ \nu(z) \\ \dfrac{1-\nu(z)}{2} \end{Bmatrix} dz, \tag{33a}$$

and

$$\left(A_{22}, B_{22}, D_{22}, B_{22}^s, D_{22}^s, H_{22}^s\right) = \left(A_{11}, B_{11}, D_{11}, B_{11}^s, D_{11}^s, H_{11}^s\right), \tag{33b}$$

$$A_{44}^s = A_{55}^s = \int_{-h/2}^{h/2} C_{44}\left[g(z)\right]^2 dz, \tag{33c}$$

3.4 Governing equations in terms of displacements

Introducing Eq. (34) into Eq. (26), the governing equations can be expressed in terms of displacements (δu_0, δv_0, δw_b, δw_s), and the appropriate equations take the form

$$\begin{aligned} &A_{11}d_{11}u_0 + A_{66}d_{22}u_0 + (A_{12}+A_{66})d_{12}v_0 - B_{11}d_{111}w_b - (B_{12}+2B_{66})d_{122}w_b \\ &\quad - (B_{12}^s + 2B_{66}^s)d_{122}w_s - B_{11}^s d_{111}w_s = 0, \end{aligned} \tag{34a}$$

$$\begin{aligned} &A_{22}d_{22}v_0 + A_{66}d_{11}v_0 + (A_{12}+A_{66})d_{12}u_0 - B_{22}d_{222}w_b - (B_{12}+2B_{66})d_{112}w_b \\ &\quad - (B_{12}^s + 2B_{66}^s)d_{112}w_s - B_{22}^s d_{222}w_s = 0, \end{aligned} \tag{34b}$$

$$\begin{aligned} &B_{11}d_{111}u_0 + (B_{12}+2B_{66})d_{122}u_0 + (B_{12}+2B_{66})d_{112}v_0 + B_{22}d_{222}v_0 \\ &\quad - D_{11}d_{1111}w_b - 2(D_{12}+2D_{66})d_{1122}w_b - D_{22}d_{2222}w_b - D_{11}^s d_{1111}w_s \\ &\quad - 2(D_{12}^s + 2D_{66}^s)d_{1122}w_s - D_{22}^s d_{2222}w_s - q = 0, \end{aligned} \tag{34c}$$

$$\begin{aligned} &B_{11}^s d_{111}u_0 + (B_{12}^s+2B_{66}^s)d_{122}u_0 + (B_{12}^s+2B_{66}^s)d_{112}v_0 + B_{22}^s d_{222}v_0 - D_{11}^s d_{1111}w_b \\ &\quad - 2(D_{12}^s+2D_{66}^s)d_{1122}w_b - D_{22}^s d_{2222}w_b - H_{11}^s d_{1111}w_s \\ &\quad - 2(H_{12}^s+2H_{66}^s)d_{1122}w_s - H_{22}^s d_{2222}w_s + A_{44}^s d_{11}w_s + A_{55}^s d_{22}w_s - q = 0 \end{aligned} \tag{34d}$$

where d_{ij}, d_{ijl} and d_{ijlm} are the following differential operators

$$d_{ij} = \frac{\partial^2}{\partial x_i \partial x_j}, \quad d_{ijl} = \frac{\partial^3}{\partial x_i \partial x_j \partial x_l}, \quad d_{ijlm} = \frac{\partial^4}{\partial x_i \partial x_j \partial x_l \partial x_m}, \quad (i, j, l, m = 1, 2). \tag{35}$$

3.5 Analytical solutions

Consider a simply supported rectangular plate with length a and width b (Fig. 3). Based on Navier solution method, the following expansions of displacements (u_0, v_0, w_b, w_s) are assumed as (Zenkour 2006)

$$\begin{Bmatrix} u_0 \\ v_0 \\ w_b \\ w_s \end{Bmatrix} = \sum_{m=1}^{\infty}\sum_{n=1}^{\infty} \begin{Bmatrix} U_{mn}\cos(\lambda\, x)\sin(\mu\, y) \\ V_{mn}\sin(\lambda\, x)\cos(\mu\, y) \\ W_{bmn}\sin(\lambda\, x)\sin(\mu\, y) \\ W_{smn}\sin(\lambda\, x)\sin(\mu\, y) \end{Bmatrix} \tag{36}$$

where U_{mn}, V_{mn}, W_{bmn}, W_{smn} unknown parameters must be determined, and $\lambda = m\pi/a$ and $\mu = n\pi/b$. The transverse load q is also expanded in the double-Fourier sine series as follows

$$q(x, y) = \sum_{m=1}^{\infty}\sum_{n=1}^{\infty} Q_{mn}\sin(\lambda\, x)\sin(\mu\, y) \tag{37}$$

The coefficients Q_{mn} are given below for some typical loads (Zenkour 2006)

$$Q_{mn} = \frac{4}{ab}\int_0^a\int_0^b q(x, y)\sin(\lambda\, x)\sin(\mu\, y)dxdy = \begin{cases} q_0 & \text{for sinusoidal load} \\ \dfrac{16 q_0}{mn\pi^2} & \text{for uniformly distributed load} \end{cases} \tag{38}$$

Substituting Eq. (37) into Eq. (35), the analytical solutions can be obtained from the matrix-vector system

$$\begin{bmatrix} a_{11} & a_{12} & a_{13} & a_{14} \\ a_{12} & a_{22} & a_{23} & a_{24} \\ a_{13} & a_{23} & a_{33} & a_{34} \\ a_{14} & a_{24} & a_{34} & a_{44} \end{bmatrix} \begin{Bmatrix} U_{mn} \\ V_{mn} \\ W_{bmn} \\ W_{smn} \end{Bmatrix} = \begin{Bmatrix} 0 \\ 0 \\ Q_{mn} \\ Q_{mn} \end{Bmatrix} \tag{39}$$

in which

$$\begin{aligned} a_{11} &= -\left(A_{11}\lambda^2 + A_{66}\mu^2\right) \\ a_{12} &= -\lambda\,\mu\left(A_{12} + A_{66}\right) \\ a_{13} &= \lambda[B_{11}\lambda^2 + (B_{12} + 2B_{66})\,\mu^2] \\ a_{14} &= \lambda[B_{11}^s\lambda^2 + (B_{12}^s + 2B_{66}^s)\,\mu^2] \\ a_{22} &= -\left(A_{66}\lambda^2 + A_{22}\mu^2\right) \\ a_{23} &= \mu[(B_{12} + 2B_{66})\,\lambda^2 + B_{22}\mu^2] \\ a_{24} &= \mu[(B_{12}^s + 2B_{66}^s)\,\lambda^2 + B_{22}^s\mu^2] \\ a_{33} &= -\left(D_{11}\lambda^4 + 2(D_{12} + 2D_{66})\lambda^2\mu^2 + D_{22}\mu^4\right) \\ a_{34} &= -\left(D_{11}^s\lambda^4 + 2(D_{12}^s + 2D_{66}^s)\lambda^2\,\mu^2 + D_{22}^s\,\mu^4\right) \\ a_{44} &= -\left(H_{11}^s\lambda^4 + 2(H_{11}^s + 2H_{66}^s)\lambda^2\mu^2 + H_{22}^s\mu^4 + A_{55}^s\lambda^2 + A_{44}^s\mu^2\right), \end{aligned} \tag{40}$$

By substituting Eq. (19) into Eq. (29) and the subsequent results into Eq. (37), the obtained stress components in terms of Young's modulus , Poisson's ratio and the unknown parameters, U_{mn}, V_{mn}, W_{bmn}, W_{smn} as follows

$$\begin{aligned} \sigma_x = \frac{E(z)}{1-\upsilon(z)^2}\sum_{m,n=1,3,5....}^{\infty}&\Big[-\left(\lambda U_{mn} + \upsilon(z)\mu V_{mn}\right) + z\left(\lambda^2 + \upsilon(z)\mu^2\right)W_{bmn} \\ &+ f(z)\left(\lambda^2 + \upsilon(z)\mu^2\right)W_{smn}\Big]\sin(\lambda x)\sin(\mu y) \end{aligned} \tag{41a}$$

Table 1 Material properties used for FGM plate

Properties	Metal aluminum Alloy 1100	Ceramic Alumina (Al_2O_3)
E (GPa)	69	380
v	0.33	0.22

$$\sigma_y = \frac{E(z)}{1-\upsilon(z)^2} \sum_{m,n=1,3,5....}^{\infty} \left[-\left(\upsilon(z)\lambda U_{mn} + \mu V_{mn}\right) + z\left(\upsilon(z)\lambda^2 + \mu^2\right) W_{bmn} + f(z)\left(\upsilon(z)\lambda^2 + \mu^2\right) W_{smn} \right] \sin(\lambda x)\sin(\mu y) \tag{41b}$$

$$\tau_{xy} = \frac{E(z)}{2\left(1+\upsilon(z)\right)} \sum_{m,n=1,3,5....}^{\infty} \left[\mu U_{mn} + \lambda V_{mn} - 2z\lambda\mu W_{bmn} - 2 f(z)\lambda\mu W_{smn}\right] \cos(\lambda x)\cos(\mu y) \tag{41c}$$

$$\tau_{xz} = \frac{E(z)}{2\left(1+\upsilon(z)\right)} \sum_{m,n=1,3,5....}^{\infty} g(z)\lambda W_{smn} \cos(\lambda x)\sin(\mu y) \tag{41d}$$

$$\tau_{yz} = \frac{E(z)}{2\left(1+\upsilon(z)\right)} \sum_{m,n=1,3,5....}^{\infty} \left[g(z)\mu W_{smn}\right] \sin(\lambda x)\cos(\mu y) \tag{41e}$$

4. Results and discussion

In order to illustrate the effect of homogenization models on stress analysis of FGM plates, various numerical examples are considered and compared for the bending and stresses responses of simply supported functionally graded plates, subjected to transverse uniform and sinusoidal loads. The material properties of FGM plates used in this study are listed in Table 1. For convenience, the following dimensionless forms are used

$$\bar{z} = \frac{z}{h}, \quad \bar{u} = \frac{10 E_c h^3}{q_0 a^4}\left(0, \frac{b}{2}, z\right),$$
$$\hat{w} = \frac{10^3 h^3 E_m}{a^4 q_0} w\left(\frac{a}{2}, \frac{b}{2}, 0\right), \quad \bar{w} = \frac{10 h^3 E_c}{a^4 q_0} w\left(\frac{a}{2}, \frac{b}{2}, 0\right)$$
$$\bar{\sigma}_x = \frac{h}{a q_0}\sigma_x\left(\frac{a}{2}, \frac{b}{2}, \frac{h}{2}\right), \quad \bar{\sigma}_{xy} = \frac{h}{a q_0}\tau_{xy}\left(0, 0, -\frac{h}{3}\right),$$
$$\bar{\tau}_{xz} = \frac{h}{a q_0}\tau_{xz}\left(0, \frac{b}{2}, 0\right) \tag{42}$$

4.1 Stress analysis of FGM plates under uniform loading

The presented refined functionally graded plate theory solution is validated through the comparison with available solutions in literatures. Table 2 presents the computed non-dimensional center point deflection of thick (*a/h*=5) simply supported functionally graded square plates subjected to a uniformly distributed load, for various values of the material index *p*. The obtained results are compared with classical and third order plate theory documented in Akbarzadeh *et al.* (2015). It should be noted that Young's modulus and Poisson's ratio are evaluated using Voigt, Reuss, Hashin Upper bounds, Hashin Lower bounds, and LRVE and Tamura models. It is evident that the present computations are in an excellent agreement with the third order plate theory solutions, the classical plate theory omits shear deformation effects, and it therefore noticeably over-estimates the deflection of thick plates. As can be seen, the obtained non-dimensional center point deflections for the ceramic phase material are lesser than those obtained for the metallic phase material and increase when material index parameter increases for all used homogenization models. As known, ceramics present a higher Young's modulus compared to metals, and consequently, the rigidity of ceramic plates can been considered more stiffener than metallic plates which involves a higher or lesser transverse deflection of the plate related to corresponding material phases, on another hand, the combination of ceramics and metals involves a marked depletion in the stiffness rigidity of the plates, in which justified this increasing of non-dimensional center point deflections for many material mixture configurations depending on material index parameter .

Table 2 Comparison of dimensionless deflection $\hat{w}$ of simply supported FGM square plate with different homogenization models (*a/h*=5) under uniform loading

p	Theory	Homogenization model					
		Voigt	Reuss	Hashin (L.B)	Hashin (U.B)	LRVE	Tamura
ceramic	CPT [(a)]	8.6209	8.6209	8.6209	8.6209	8.6209	8.6209
	TSDT [(a)]	9.9796	9.9796	9.9796	9.9796	9.9796	9.9796
	Present SSDT	9.9845	9.9845	9.9845	9.9845	9.9845	9.9845
0.5	CPT [(a)]	13.0495	19.3436	16.9256	14.6739	16.6468	16.5749
	TSDT [(a)]	14.9113	22.3403	19.4628	16.7373	19.0247	18.9980
	Present SSDT	14.9134	22.3567	19.4733	16.7418	19.0340	19.0069
1	CPT [(a)]	16.8376	23.1595	20.9825	18.7196	20.8721	20.6500
	TSDT [(a)]	19.1894	27.2708	24.4424	21.4247	24.1483	23.9452
	Present SSDT	19.1998	27.3029	24.4676	21.4392	24.1719	23.9682
2	CPT [(a)]	21.4493	26.4230	24.6096	22.8888	24.4164	24.3500
	TSDT [(a)]	24.7938	32.0171	29.5094	26.7988	29.2035	29.0630
	Present SSDT	24.8204	32.0660	29.5570	26.8349	29.2568	29.1099
10	CPT [(a)]	27.6679	33.9279	31.5664	29.3179	31.2264	31.2192
	TSDT [(a)]	34.9869	41.7976	39.3203	36.8419	38.9849	38.9400
	Present SSDT	35.0516	41.8423	39.3541	36.8894	39.0140	38.9753
Metal	CPT [(a)]	44.4589	44.4589	44.4589	44.4589	44.4589	44.4589
	TSDT [(a)]	52.7839	52.7839	52.7839	52.7839	52.7839	52.7839
	Present SSDT	52.8099	52.8099	52.8099	52.8099	52.8099	52.8099

[(a)] Given by Akbarzadeh *et al.* (2015)

The comparison between solutions generated with different homogenization models shows important differences in computed non-dimensional center point deflection values. Maximum values obtained of non-dimensional center point deflection correspond to Reuss's model which estimates the effective proprieties provided by the lower bounds. Minimum obtained values are produced by Voigt's model which provides approximate estimation of the effective proprieties based on upper bounds. Hashin's upper bounds model estimates the effective proprieties

Table 3 Comparison of dimensionless deflection $\hat{w}$ of simply supported FGM square plate with different homogenization models (a/h=10) under uniform loading

p		Homogenization model					
		Voigt	Reuss	Hashin (L.B)	Hashin (U.B)	LRVE	Tamura
ceramic	CPT [(a)]	8.6209	8.6209	8.6209	8.6209	8.6209	8.6209
	TSDT [(a)]	8.8105	8.8105	8.8105	8.8105	8.8105	8.8105
	Present SSDT	8.8142	8.8142	8.8142	8.8142	8.8142	8.8142
0.5	CPT [(a)]	13.0495	19.3436	16.9256	14.6739	16.6468	16.5749
	TSDT [(a)]	13.2870	19.7509	17.2617	14.9324	16.9479	16.8889
	Present SSDT	13.2876	19.7594	17.2671	14.9348	16.9535	16.8937
1	CPT [(a)]	16.8376	23.1595	20.9825	18.7196	20.8721	20.6500
	TSDT [(a)]	17.1282	23.7772	21.4750	19.0641	21.3197	21.1072
	Present SSDT	17.1354	23.7929	21.4877	19.0730	21.3320	21.1192
2	CPT [(a)]	21.4493	26.4230	24.6096	22.8888	24.4164	24.3500
	TSDT [(a)]	21.9014	27.3563	25.3981	23.4578	25.1790	25.0960
	Present SSDT	21.9146	27.3789	25.4185	23.4741	25.2006	25.1160
10	CPT [(a)]	27.6679	33.9279	31.5664	29.3179	31.2263	31.2192
	TSDT [(a)]	29.0130	35.3068	32.9562	30.6876	32.6231	32.6065
	Present SSDT	29.0405	35.3510	32.9849	30.7133	32.6484	32.6342
Metal	CPT [(a)]	44.4589	44.4589	44.4589	44.4589	44.4589	44.4589
	TSDT [(a)]	45.7670	45.7670	45.7670	45.7670	45.7670	45.7670
	Present SSDT	45.7863	45.7863	45.7863	45.7863	45.7863	45.7863

[(a)] Given by Akbarzadeh *et al.* (2015)

Table 4 Comparison of dimensionless deflection $\hat{w}$ of simply supported FGM square plate with different homogenization models (a/h=100) under uniform loading

p		Homogenization model					
		Voigt	Reuss	Hashin (L.B)	Hashin (U.B)	LRVE	Tamura
ceramic	CPT [(a)]	8.6209	8.6209	8.6209	8.6209	8.6209	8.6209
	TSDT [(a)]	8.4241	8.4241	8.4241	8.4241	8.4241	8.4241
	Present SSDT	8.4272	8.4272	8.4272	8.4272	8.4272	8.8142
0.5	CPT [(a)]	13.0495	19.3436	16.9256	14.6739	16.6468	16.5749
	TSDT [(a)]	12.7502	18.8949	16.5342	14.3359	16.2616	16.1918
	Present SSDT	12.7501	18.9001	16.5375	14.3373	16.2654	16.1947
1	CPT [(a)]	16.8376	23.1595	20.9825	18.7196	20.8721	20.6500
	TSDT [(a)]	16.4470	22.6221	20.4940	18.2838	20.3847	20.1690
	Present SSDT	16.4527	22.6314	20.5017	18.2904	20.3924	20.1767
2	CPT [(a)]	21.4493	26.4230	24.6096	22.8888	24.4164	24.3500
	TSDT [(a)]	20.9452	25.8149	24.0385	22.3531	23.8481	23.7842
	Present SSDT	20.9532	25.8275	24.0487	22.3620	23.8580	23.7941
10	CPT [(a)]	27.6679	33.9279	31.5664	29.3179	31.2263	31.2192
	TSDT [(a)]	27.0369	33.1600	30.8511	28.6518	30.5188	30.5116
	Present SSDT	27.0500	33.2024	30.8763	28.6684	30.5410	30.5351
Metal	CPT [(a)]	44.4589	44.4589	44.4589	44.4589	44.4589	44.4589
	TSDT [(a)]	43.4475	43.4475	43.4475	43.4475	43.4475	43.4475
	Present SSDT	43.4630	43.4630	43.4630	43.4630	43.4630	43.4630

[(a)] Given by Akbarzadeh *et al.* (2015)

based on optimal shear and bulk modulus for upper phase material, which explains the close values of the obtained results with Voigt's model. For Hashin's lower bounds, LRVE and Tamura models, the effective proprieties are derived as functions of the lower phase material, manifesting in closely correlating values for center point deflection. As mentioned above, both Tamura and LRVE models use the same Poisson's ratio estimation and this generates very close results.

Next FGM plates with thickness ratio a/h=10 are analysed, another situation of relevance to aircraft and spacecraft structures. In this scenario, the accuracy of present theory and the effect of homogenization models are examined and discussed for moderately FGM thick plates. This example aims to predict the non-dimensional center point deflection for moderately thick plates under uniformly load; the obtained results are compared with CPT and those predicted by third order plate theory in Table 3. It is observed that non-dimensional center point deflections are slight lesser compared to thick FGM plates; it is due to reduce effect of shear deformations through the plate thickness. The lesser values of non-dimensional center point deflections are observed in the ceramic rich phase and increase to higher magnitudes in the metallic rich phase. The obtained results demonstrate that the same accuracy is achievable with the present theory using a lower number of unknowns than third order theory used by Akbarzadeh *et al.* (2015), since the classical plate theory neglects the shear deformation effects, it under-estimates center point deflection of FGM plates with important thickness ratio .

Additionally, and from a comparison of dimensionless center point deflections obtained with used homogenization models, the effect of homogenization models does not depend on the thickness ratio of plate; the assumptions of purposed homogenisation involve this difference in predicting the non-dimensional center point deflection of FGM plates.

The last validation example is performed for thin FGM square plates. Table 4 indicates that the present results are in very good agreement with both classical and third order plate theories for different values of material index parameter. The present theory and *third order plate theory* achieve almost identical results; nevertheless, this latter theory contains a greater number of unknowns than those associated with the present theory. However, the classical plate theory neglects the effect of shear deformation; this effect is not significant in bending analysis of thin plates. Examination of Table 4 also reveals that for all used homogenization models, the non-dimensional center point deflections increase from the ceramic rich phase to metallic rich phase as material index parameter increases. The comparison of used homogenization models shows that the obtained results vary from model to another. However, the difference between maximum values obtained by Reuss's model and minimum values obtained by Voigt's model is relatively reduced compared to thick and moderately thick FGM plates, it is due to the transverse shear stiffness contribution related to thin plates which has been reduced

Table 5 Comparison of dimensionless stresses of simply supported FGM square plate with different homogenization models (a/h=10) under uniform loading

p	Stresses	Homogenization model					
		Voigt	Reuss	Hashin (L.B)	Hashin (U.B)	LRVE	Tamura
Ceramic	$\bar{\sigma}_x$	2.7132	2.7130	2.7130	2.7132	2.7132	2.7130
	$\bar{\sigma}_{xy}$	1.4327	1.4327	1.4327	1.4327	1.4327	1.4327
	$\bar{\tau}_{xz}$	0.5130	0.5130	0.5130	0.5130	0.5130	0.5130
0.5	$\bar{\sigma}_x$	3.5185	4.6376	4.1916	3.7982	4.1227	4.1290
	$\bar{\sigma}_{xy}$	1.2943	1.1417	1.1511	1.2603	1.1681	1.1758
	$\bar{\tau}_{xz}$	0.5245	0.4857	0.5007	0.5177	0.5066	0.5042
1	$\bar{\sigma}_x$	4.1257	5.3897	4.8816	4.4457	4.8018	4.8116
	$\bar{\sigma}_{xy}$	1.1065	1.0534	1.0381	1.0847	1.0278	1.0459
	$\bar{\tau}_{xz}$	0.5111	0.4650	0.4745	0.4953	0.4745	0.4774
2	$\bar{\sigma}_x$	4.8023	6.2836	5.6327	5.1272	5.4976	5.5476
	$\bar{\sigma}_{xy}$	0.9608	1.0256	1.0003	0.9829	0.9953	0.9981
	$\bar{\tau}_{xz}$	0.4675	0.4538	0.4495	0.4541	0.4398	0.4485
10	$\bar{\sigma}_x$	6.7085	9.4972	8.4539	7.4531	8.3130	8.2997
	$\bar{\sigma}_{xy}$	1.0271	1.0943	1.0672	1.0432	1.0618	1.0633
	$\bar{\tau}_{xz}$	0.4545	0.4865	0.4790	0.4663	0.4794	0.4773
Metal	$\bar{\sigma}_x$	14.006	14.006	14.006	14.006	14.006	14.006
	$\bar{\sigma}_{xy}$	1.2287	1.2287	1.2287	1.2287	1.2287	1.2287
	$\bar{\tau}_{xz}$	0.5125	0.5125	0.5125	0.5125	0.5125	0.5125

(i.e., involving to neglect the effect of shear deformations).

After this validation for predicting the center point deflection of FGM plates subject to uniformly loads, this segment is accomplished with presenting the effect of homogenization models on the in-plane and shear stresses of thus plates. Table 5 contains dimensionless stresses of simply supported FGM plates under uniformly load with thickness ratio a/h=10 and various values of material index parameter. It is seen from the Table 5 that the dimensionless axial stress $\bar{\sigma}_x$ increases with the increasing value of material index parameter, lower values of dimensionless axial stress $\bar{\sigma}_x$ is observed for fully ceramic plate and higher values for fully metal plate, this is justified by the higher Young's modulus of used ceramic material compared to metallic Young's modulus. It is clearly that the difference between minimum values obtained by Voigt's model and the maximum values obtained by Reuss's model is more significant and increases when material index parameter increases. Hashin's lower bounds, LRVE and Tamura models present a closely correlating values for dimensionless axial stress. As mentioned above, both Tamura and LRVE models use the same Poisson's ratio estimation and this generates very close results. The dimensionless longitudinal tangential stress $\bar{\sigma}_{xy}$ decreases with the increasing value of material index parameter, up to phase transforming to fully homogeneous metal material in which gives the relatively same as that for a fully ceramic

Table 6 Comparison of dimensionless deflection $\bar{w}$ of simply supported FGM square plate with various (a/h) ratio and different homogenization models under sinusoidal loading

a/h	p	Homogenization model					
		Voigt	Reuss	Hashin (L.B)	Hashin (U.B)	LRVE	Tamura
5	ceramic	0.35214	0.35214	0.35214	0.35214	0.35214	0.35214
	0.5	0.52546	0.78840	0.68650	0.58978	0.67069	0.66989
	1	0.67640	0.96416	0.86336	0.75550	0.85254	0.84549
	2	0.87534	1.1346	1.0451	0.94726	1.0343	1.0290
	10	1.2437	1.4821	1.3949	1.3084	1.3831	1.3817
	metal	1.8659	1.8659	1.8659	1.8659	1.8659	1.8659
10	ceramic	0.30787	0.30787	0.30787	0.30787	0.30787	0.30787
	0.5	0.46394	0.69016	0.60306	0.52147	0.59200	0.58995
	1	0.59831	0.83144	0.75069	0.66603	0.74510	0.73773
	2	0.76547	0.95737	0.88867	0.82019	0.88099	0.87799
	10	1.0167	1.2366	1.1542	1.0749	1.1425	1.1420
	metal	1.6003	1.6003	1.6003	1.6003	1.6003	1.6003
100	ceramic	0.29322	0.29322	0.29322	0.29322	0.29322	0.29322
	0.5	0.44361	0.65763	0.57543	0.49886	0.56597	0.56350
	1	0.57243	0.78747	0.71337	0.63642	0.70954	0.70205
	2	0.72899	0.89866	0.83680	0.77801	0.83015	0.82791
	10	0.94122	1.1553	1.0744	0.99754	1.0627	1.0625
	metal	1.5123	1.5123	1.5123	1.5123	1.5123	1.5123

Table 7 Comparison of dimensionless stresses of simply supported FGM square plate with different homogenization models (a/h=10) under sinusoidal loading

p		Homogenization model					
		Voigt	Reuss	Hashin (L.B)	Hashin (U.B)	LRVE	Tamura
ceramic	$\bar{\sigma}_x$	1.8708	1.8708	1.8708	1.8708	1.8708	1.8708
	$\bar{\sigma}_{xy}$	0.78755	0.78755	0.78755	0.78755	0.78755	.78755
	$\bar{\tau}_{xz}$	0.24622	0.24622	0.24622	0.24622	0.24622	.24622
0.5	$\bar{\sigma}_x$	2.4268	3.2001	2.8921	2.6200	2.8441	2.8487
	$\bar{\sigma}_{xy}$	0.70962	0.62684	0.63167	0.69110	0.64078	0.64511
	$\bar{\tau}_{xz}$	0.25148	0.23354	0.24048	0.24802	0.24324	0.24189
1	$\bar{\sigma}_x$	2.8462	3.7202	3.3692	3.0673	3.3138	3.3208
	$\bar{\sigma}_{xy}$	0.60684	0.57915	0.57031	0.59529	0.56454	0.57443
	$\bar{\tau}_{xz}$	0.24528	0.22365	0.22809	0.23787	0.22811	0.22950
2	$\bar{\sigma}_x$	3.3150	4.3385	3.8899	3.5397	3.7966	3.8310
	$\bar{\sigma}_{xy}$	0.52770	0.56470	0.55052	0.54034	0.54778	0.54915
	$\bar{\tau}_{xz}$	0.22472	0.21838	0.21634	0.21878	0.21188	0.21595
10	$\bar{\sigma}_x$	4.6348	6.5545	5.8356	5.1462	5.7382	5.7297
	$\bar{\sigma}_{xy}$	0.56656	0.60324	0.58849	.57532	0.58554	0.58637
	$\bar{\tau}_{xz}$	0.21921	0.23443	0.23098	.22481	0.23108	0.23010
Metal	$\bar{\sigma}_x$	9.6623	9.6624	9.6624	9.6624	9.6624	9.6624
	$\bar{\sigma}_{xy}$	0.67614	0.67614	0.67614	0.67614	0.67614	0.67614
	$\bar{\tau}_{xz}$	0.24617	0.24617	0.24617	0.24617	0.24617	0.24617

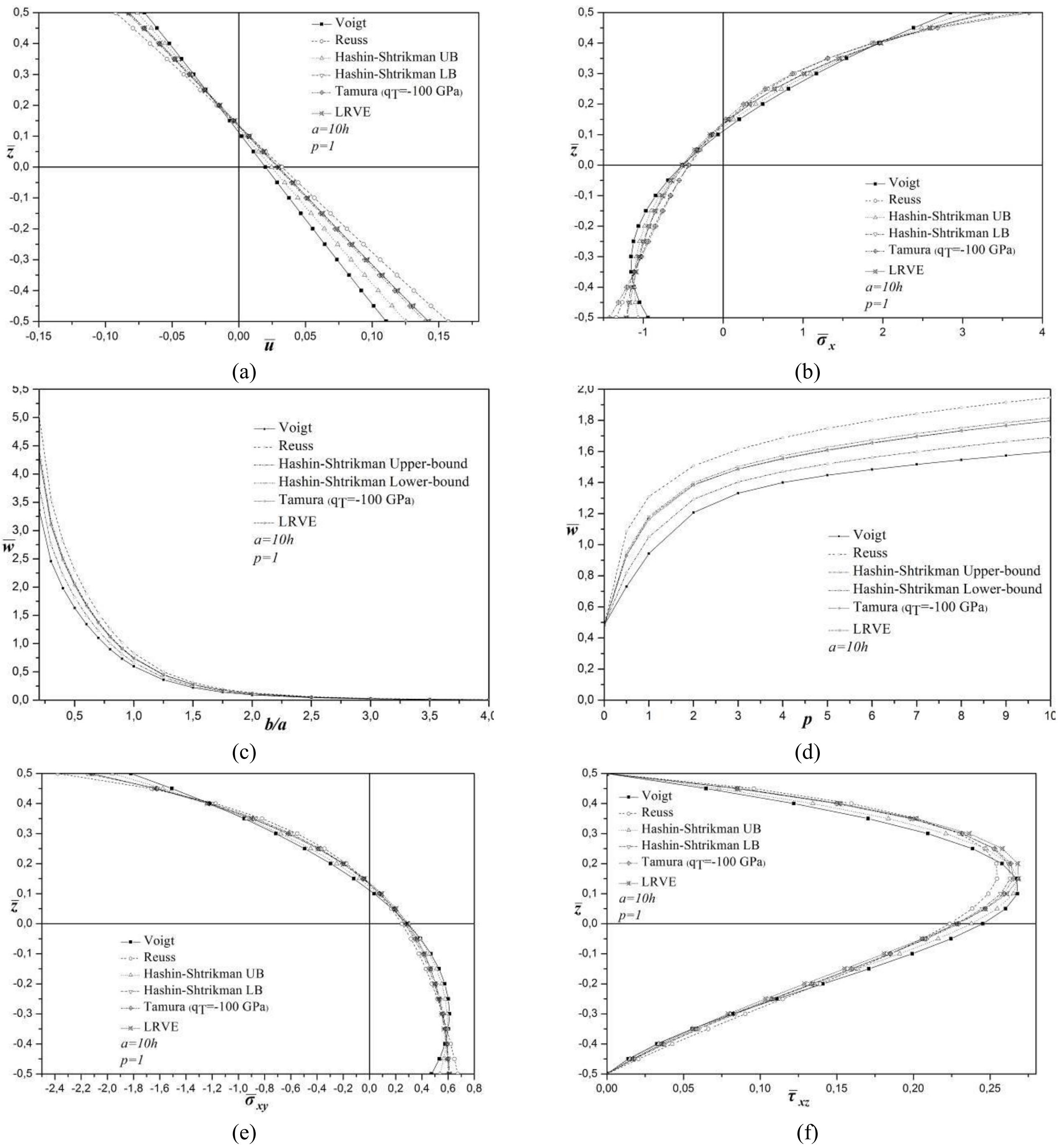

Fig. 4 Variation of dimensionless displacement and stresses through the thickness of FGM square plates (*a*/*h*=10, *p*=1) under sinusoidal load: (a) the axial displacement $\bar{u}$, (b) the axial stress $\bar{\sigma}_x$ (c) the deflection $\bar{w}$ as a function of the aspect ratio (b/a), (d) the deflection $\bar{w}$ as a function of the material index parameter *p*, (e) the longitudinal shear stress $\bar{\sigma}_{xy}$, (f) the transversal shear stress $\bar{\tau}_{xz}$

plate, this is because the dimensionless stresses do not depend on the value of the elasticity modulus excepting the Poisson's ratio. There is no important difference between used homogenization models in obtained dimensionless transversal shear stress $\bar{\tau}_{xz}$ values.

4.2 Stress analysis of FGM plates under sinusoidal loading

As it is well known, the displacement and stress magnitudes are over-predicted by applying the uniformly loads, new results for stress analysis of FGM plates with using various homogenization models are also presented for sinusoidal load cases. Table 6 shows the effect of material index parameter and thickness aspect ratio *a/h* on the dimensionless deflection $\bar{w}$ of simply supported FGM square plates under sinusoidal loading, by using the Voigt, Reuss and Hashin Upper bounds, Hashin Lower bounds, LRVE and Tamura models. Inspection of Table 6 shows that the dimensionless deflections increase with the increasing value of material index parameter, it is marked also that the margin of difference between the maximum values given by Reuss's model and the minimum values given by Voigt's model decreases with the increasing value of material index parameter.

On the other hand, Table 7 presents the effect of material index parameter on dimensionless stresses of simply supported FGM square plate with thickness ratio a/h=10 using Voigt, Reuss and Hashin Upper bounds, Hashin Lower bounds, LRVE and Tamura models. As can be seen, the obtained non-dimensional stresses for the ceramic phase material are lower than those obtained for the metallic phase material and increase when material index parameters increase for all the homogenization models. It is also observed that the difference between maximum values obtained by Reuss's model and the minimum values obtained by Voigt's model is more significant and decreases when material index parameter increases.

In order to highlight the effect of homogenization models on axial displacement, Fig. 4(a) shows the distributions of dimensionless axial displacement $\bar{u}$ through the thickness of an FGM plate under sinusoidal loading with thickness ratio a/h=10 and material index parameter p=1. A careful examination of the Fig. 4(a) shows that the distribution of the dimensionless axial displacement trough the plate thickness has two distinct regions, the negative maximum displacement presents the axial displacement due to compressive strain which obtained at the top of plate surface and the positive maximum displacement presents the axial displacement due to tensile strain obtained at the bottom of plate, and change with the increase of side-to-thickness ratio from metal to ceramic surfaces. It is observed also that maximum differences for dimensionless axial displacement of used homogenization models are given in the both upper and lower surfaces of the plate.

The Figs. 4(c)-(d) show the variation of the dimensionless center point deflection with the aspect ratio (b/a) and material index parameter respectively, It is observed that the obtained dimensionless center point deflection decreases when the aspect ratio, b/a, is increased for all models and the margin of the difference between computed dimensionless center point deflection generated with the used homogenization models decreases as the aspect ratio b/h increases. The presented dimensionless center point deflection is higher for the metal phase material and lower for the ceramic phase material and increases as the material index parameter increases. It is also observed that the difference between maximum values obtained by Reuss's model and the minimum values obtained by Voigt's model increases when material index parameter increases. As illustrated in Figs. 4(c)-(d), Hashin lower bounds , Tamura and LRVE models present a closely correlation of dimensionless center point deflection.

The distribution of dimensionless axial stress $\bar{\sigma}_x$ across the thickness is illustrated in Fig. 4(b), it can be seen that the dimensionless axial stress presents two different magnitudes trough the thickness of plate, negative and positive in the bottom and top surfaces of the plate, respectively.

Likewise, the negative stress is corresponded to compressive stress in which the maximum magnitude is situated on the bottom of plate; the positive stress is corresponded to tensile stress and the top surface of plate which presents the maximum magnitudes. Contrary to axial stress, the tensile and compressive values of longitudinal tangential stress $\bar{\sigma}_{xy}$ (Fig. 4(e)), are situated on the top and bottom surfaces of the plate, respectively. It can be observed that the difference between dimensionless stresses generated by used homogenization models is important at top and bottom surfaces of plate, and a relatively slight difference is observed while the top surface transforms from the metal-rich to the bottom ceramic-rich surface of plate. Fig. 4(f) shows the distribution of dimensionless transverse shear stress $\bar{\tau}_{xz}$ across the plate thickness by aforementioned homogenization models; it is clearly that free surface conditions at the top and bottom surfaces of the plates are naturally satisfied. However, the influence of inhomogeneity governed by the material index parameter has significant effect on transvers shear stress distribution through the plate thickness, it can be noticed that in the isotropic case, the maximum magnitude of shear stress occurs at the plate center. It can be also observed that the stresses generated by used homogenization models carry slightly more difference than in-plan stresses, because the shears stiffness terms are reduced compared to both membrane and bending stiffness terms. Moreover, the maximum magnitudes of dimensionless transverse shear stress obtained by used homogenization models are very closely and the differences are relatively insignificant.

5. Conclusions

In the present study, the effect of various homogenization models is presented for stress analyses of functionally graded material (FGM) plates. The present refined plate theory has been formulated on the assumption that displacement field vary as a sinusoidal function across the plate thickness without requiring any shear correction factors, as the present refined theory naturally satisfies the shear stress free condition at the top and bottom surfaces of the plate. By dividing the transverse displacement into bending and shear components, the number of unknowns and governing equations emerging in the present theory is reduced to four, and this refined theory is therefore somewhat simpler than alternate theories available in the scientific literature. The governing equations are derived from the principle of virtual displacements and solved analytically via Navier's method to compute the stresses and displacements of simply supported plate under two different load cases, uniform and sinusoidal distribution loads. The obtained results have been compared with the published results of other theories. Additionally, the effect of homogenization models has been investigated and their impact on stress behaviour of FGM plates is also presented. The key conclusions that emerge from the present numerical results can be highlighted as follows:

1. The homogenization model is considered as an important procedure to study the interaction between composite material constituents at microscopic-scale, whereas the transition from micro-scale to macro-scale emphasizes technological applications to the analysis and design of structures. This procedure is conducted by using micromechanics models to describe correctly the mechanical response of FGM plates. Through the presented comparative study, it can be concluded that the effect of homogenization models is non-trivial in predicting the displacement and stresses of functionally graded plates.

2. The Most of papers in the literature on FGMs analysis use the Voigt's model to analyze the mechanical behaviors of FGM plates. Therefore, this model is accurate only for FGM with relatively closer elastic proprieties such as Poisson's ratio. So, it is necessary to explore alternative homogenization models such as Voigt, Reuss and Hashin Upper/Lower bounds, LRVE and Tamura models. Hence, the comparison between these models shows that for same homogeneous material phase the agreement is identical, but for the inhomogeneity phase there is some discrepancy since each model is based on different assumptions and specific criteria.

3. For dimensionless deflections, the minimum magnitudes are obtained by Voigt's model and the maximum magnitudes are given by Reuss's model, because the both models estimate the effective proprieties based on upper and lower bounds which corresponded to ceramic and metal material phases respectively. Since the effective proprieties are determined by using the bulk and shear modulus for upper and lower bounds, the margin of difference is reduced using Hashin-Strickman's models. Tamura's model derives effective properties from a modification of the Voigt's model which includes an empirical fitting parameter q_T based on the nature of matrix-inclusions phases. This model is considered as a correction factor to Voigt model. The LRVE model takes into account the small cellular mechanical properties to predict the effective proprieties at the macroscopic-scale for two phase materials and it is generally used for random distribution materials or interphase regions of composites.

4. For stresses analysis, the presented figures show that the inhomogeneity phases present an important factor in stress distributions through the plate thickness. The assumptions and specific criteria of each model lead to significant deviation in stress distributions.

5. It is observed that increasing material index parameter increases both center point deflection and axial stresses, contrary to both longitudinal tangential and shear stresses decrease when this parameter increases.

6. The results for FGM plates under sinusoidal load serve as benchmark results for future comparisons.

In light of this investigation presented herein, many other suggestions of future trends can be stated here. The most of important additional contributions are to extend this study for others investigations such as dynamic, buckling and damage responses of FGM plates. The missing experimental data present a good motivation to validate the homogenization models considered to establish the optimum choice for functionally graded plate problems. Also another possible extension of the current work is to consider micro-structural material behaviour which could be simulated within the framework of Eringen's micropolar elastic models for both static and dynamic loading (Othman *et al.* 2013) with different homogenization models presented in this study. Finally, it is also interesting to consider recent development continuum models (Karami *et al.* 2017b, 2018d, e) to investigate the mechanical behaviour of FG structures more complex geometrical configurations.

References

Abdelaziz, H.H., Ait Amar Meziane, M., Bousahla, A.A., Tounsi, A., Mahmoud, S.R. and Alwabli, A.S. (2017), "An efficient hyperbolic shear deformation theory for bending, buckling and free vibration of FGM sandwich plates with various boundary conditions", *Steel Compos. Struct.*, **25**(6), 693-704.

Abualnour, M., Houari, M.S.A., Tounsi, A., Adda Bedia, E.A. and Mahmoud, S.R. (2018), "A novel quasi-3D trigonometric plate theory for free vibration analysis of advanced composite plates", *Compos. Struct.*, **184**, 688-697.

Ahouel, M., Houari, M.S.A., Adda Bedia, E.A. and Tounsi, A. (2016), "Size-dependent mechanical behavior of functionally graded trigonometric shear deformable nanobeams including neutral surface position concept", *Steel Compos. Struct.*, **20**(5), 963-981.

Ait Amar, M.M., Abdelaziz, H.H. and Tounsi, A. (2014), "An efficient and simple refined theory for buckling and free vibration of exponentially graded sandwich plates under various boundary conditions", *J. Sandw. Struct. Mater.*, **16**(3), 293-318.

Ait Atmane, H., Tounsi, A., Bernard, F. and Mahmoud, S.R. (2015), "A computational shear displacement model for vibrational analysis of functionally graded beams with porosities", *Steel Compos. Struct.*, **19**(2), 369-384.

Ait Yahia, S., Ait Atmane, H., Houari, M.S.A. and Tounsi, A. (2015), "Wave propagation in functionally graded plates with porosities using various higher-order shear deformation plate theories", *Struct. Eng. Mech.*, **53**(6), 1143-1165.

Akavci, S.S. and Tanrikulu, A.H. (2015), "Static and free vibration analysis of functionally graded plates based on a new quasi-3D and 2D shear deformation theories", *Compos. Part B*, **83**, 203-215.

Akbarzadeh, A.H., Abedini, A. and Chen, Z.T. (2015), "Effect of micromechanical models on structural responses of functionally graded plates", *Compos. Struct.*, **119**, 598-609.

Aldousari, S.M. (2017), "Bending analysis of different material distributions of functionally graded beam", *Appl. Phys. A*, **123**, 296.

Al-Basyouni, K.S., Tounsi, A. and Mahmoud, S.R. (2015), "Size dependent bending and vibration analysis of functionally graded micro beams based on modified couple stress theory and neutral surface position", *Compos. Struct.*, **125**, 621-630.

Arani, A.J. and Kolahchi, R. (2016), "Buckling analysis of embedded concrete columns armed with carbon nanotubes", *Comput. Concrete*, **17**(5), 567-578.

Amnieh, H.B., Zamzam, M.S. and Kolahchi, R. (2018), "Dynamic analysis of non-homogeneous concrete blocks mixed by SiO2 nanoparticles subjected to blast load experimentally and theoretically", *Constr. Build. Mater.*, **174**, 633-644.

Attia, A., Tounsi, A., Adda Bedia, E.A. and Mahmoud, S.R. (2015), "Free vibration analysis of functionally graded plates with temperature-dependent properties using various four variable refined plate theories", *Steel Compos. Struct.*, **18**(1), 187-212.

Attia, A., Bousahla, A.A., Tounsi, A., Mahmoud, S.R. and Alwabli, A.S. (2018), "A refined four variable plate theory for thermoelastic analysis of FGM plates resting on variable elastic foundations", *Struct. Eng. Mech.*, **65**(4), 453-464.

Bachir Bouiadjra, R., Mahmoudi, A., Benyoucef, S., Tounsi, A. and Bernard, F. (2018), "Analytical investigation of bending response of FGM plate using a new quasi 3D shear deformation theory: Effect of the micromechanical models", *Struct. Eng. Mech.*, **66**(3), 317-328.

Bakhadda, B., Bachir Bouiadjra, M., Bourada, F., Bousahla, A.A., Tounsi, A. and Mahmoud, S.R. (2018), "Dynamic and bending analysis of carbon nanotube-reinforced composite plates with elastic foundation", *Wind Struct.*, Accepted.

Bakora, A. and Tounsi, A. (2015), "Thermo-mechanical post-buckling behavior of thick functionally graded plates resting on elastic foundations", *Struct. Eng. Mech.*, **56**(1), 85-106.

Barati, M.R. and Shahverdi, H. (2016), "A four-variable plate theory for thermal vibration of embedded FG nanoplates under non-uniform temperature distributions with different boundary conditions", *Struct. Eng. Mech.*, **60**(4), 707-727.

Behravan Rad, A. (2012), "Static response of 2-D functionally graded circular plate with gradient thickness and elastic foundations to compound loads", *Struct. Eng. Mech.*, **44**(2), 139-161.

Belabed, Z., Houari, M.S.A., Tounsi, A., Mahmoud, S.R. and Anwar Bég, O. (2014), "An efficient and simple higher order shear and normal deformation theory for functionally graded material (FGM) plates", *Compos. Part B*, **60**, 274-283.

Belabed, Z., Bousahla, A.A., Houari, M.S.A., Tounsi, A. and Mahmoud, S.R. (2018), "A new 3-unknown hyperbolic shear deformation theory for vibration of functionally graded sandwich plate", *Earthq. Struct.*, **14**(2), 103-115.

Beldjelili, Y., Tounsi, A. and Mahmoud, S.R. (2016), "Hygrothermo- mechanical bending of S-FGM plates resting on variable elastic foundations using a four-variable trigonometric plate theory", *Smart Struct. Syst.*, **18**(4), 755-786.

Belkorissat, I., Houari, M.S.A., Tounsi, A., Adda Bedia, E.A. and Mahmoud, S.R. (2015), "On vibration properties of functionally graded nano-plate using a new nonlocal refined four variable model", *Steel Compos. Struct.*, **18**(4), 1063-1081.

Bellifa, H., Benrahou, K.H., Hadji, L., Houari, M.S.A. and Tounsi, A. (2016), "Bending and free vibration analysis of functionally graded plates using a simple shear deformation theory and the concept the neutral surface position", *J. Braz. Soc. Mech. Sci. Eng.*, **38**(1), 265-275.

Bellifa, H., Bakora, A., Tounsi, A., Bousahla, A.A. and Mahmoud, S.R. (2017a), "An efficient and simple four variable refined plate theory for buckling analysis of functionally graded plates", *Steel Compos. Struct.*, **25**(3), 257-270.

Bellifa, H., Benrahou, K.H., Bousahla, A.A., Tounsi, A. and Mahmoud, S.R. (2017b), "A nonlocal zeroth-order shear deformation theory for nonlinear postbuckling of nanobeams", *Struct. Eng. Mech.*, **62**(6), 695-702.

Benadouda, M., Ait Atmane, H., Tounsi, A., Bernard, F. and Mahmoud, S.R. (2017), "An efficient shear deformation theory for wave propagation in functionally graded material beams with porosities", *Earthq. Struct.*, **13**(3), 255-265.

Benchohra, M., Driz, H., Bakora, A., Tounsi, A., Adda Bedia, E.A. and Mahmoud, S.R. (2018), "A new quasi-3D sinusoidal shear deformation theory for functionally graded plates", *Struct. Eng. Mech.*, **65**(1), 19-31.

Bennoun, M., Houari, M.S.A. and Tounsi, A. (2016), "A novel five variable refined plate theory for vibration analysis of functionally graded sandwich plates", *Mech. Adv. Mater. Struct.*, **23**(4), 423-431.

Besseghier, A., Houari, M.S.A., Tounsi, A. and Mahmoud, S.R. (2017), "Free vibration analysis of embedded nanosize FG plates using a new nonlocal trigonometric shear deformation theory", *Smart Struct. Syst.*, **19**(6), 601-614.

Bilouei, B.S., Kolahchi, R. and Bidgoli, M.R. (2016), "Buckling of concrete columns retrofitted with nano-fiber reinforced polymer (NFRP)", *Comput. Concrete*, **18**(5), 1053-1063.

Birman, V. and Byrd, LW. (2007), "Modeling and analysis of functionally graded materials and structures", *ASME Appl. Mech. Rev.*, **60**(5), 195-216.

Bouafia, K., Kaci, A., Houari, M.S.A., Benzair, A. and Tounsi, A. (2017), "A nonlocal quasi-3D theory for bending and free flexural vibration behaviors of functionally graded nanobeams", *Smart Struct. Syst.*, **19**(2), 115-126.

Bouderba, B., Houari, M.S.A. and Tounsi, A. (2013), "Thermomechanical bending response of FGM thick plates resting on Winkler-Pasternak elastic foundations", *Steel Compos. Struct.*, **14**, 85-104.

Bouderba, B., Houari, M.S.A. and Tounsi, A. and Mahmoud, S.R. (2016), "Thermal stability of functionally graded sandwich plates using a simple shear deformation theory", *Struct. Eng. Mech.*, **58**(3), 397-422.

Bouhadra, A., Tounsi, A., Bousahla, A.A., Benyoucef, S. and Mahmoud, S.R. (2018), "Improved HSDT accounting for effect of thickness stretching in advanced composite plates", *Struct. Eng. Mech.*, **66**(1), 61-73.

Boukhari, A., Ait Atmane, H., Tounsi, A., Adda Bedia, E.A. and Mahmoud, S.R. (2016), "An efficient shear deformation theory for wave propagation of functionally graded material plates", *Struct. Eng. Mech.*, **57**(5), 837-859.

Bounouara, F., Benrahou, K.H., Belkorissat, I. and Tounsi, A. (2016), "A nonlocal zeroth-order shear deformation theory for free vibration of functionally graded nanoscale plates resting on elastic foundation", *Steel Compos. Struct.*, **20**(2), 227-249.

Bourada, M., Kaci, A., Houari, M.S.A. and Tounsi, A. (2015), "A new simple shear and normal deformations theory for functionally graded beams", *Steel Compos. Struct.*, **18**(2), 409-423.

Bousahla, A.A., Houari, M.S.A., Tounsi, A. and Adda Bedia, E.A. (2014), "A novel higher order shear and normal deformation theory based on neutral surface position for bending analysis of advanced composite plates", *Int. J. Comput. Meth.*, **11**(6), 1350082.

Bousahla, A.A., Benyoucef, S. Tounsi, A. and Mahmoud, S.R. (2016), "On thermal stability of plates with functionally graded coefficient of thermal expansion", *Struct. Eng. Mech.*, **60**(2), 313-335.

Chikh, A., Tounsi, A., Hebali, H. and Mahmoud, S.R. (2017), "Thermal buckling analysis of cross-ply laminated plates using a simplified HSDT", *Smart Struct. Syst.*, **19**(3), 289-297.

Cho, J.R. and Ha, D.Y. (2001), "Averaging and finite-element discretization approaches in the numerical analysis of functionally graded materials", *Mater. Sci. Eng.*, **302**(2), 187-196.

Draiche, K., Tounsi, A. and Mahmoud, S.R. (2016), "A refined theory with stretching effect for the flexure analysis of laminated composite plates", *Geomech. Eng.*, **11**(5), 671-690.

El-Haina, F., Bakora, A., Bousahla, A.A., Tounsi, A. and Mahmoud, S.R. (2017), "A simple analytical approach for thermal buckling of thick functionally graded sandwich plates", *Struct. Eng. Mech.*, **63**(5), 585-595.

Fahsi, A., Tounsi, A., Hebali, H., Chikh, A., Adda Bedia, E.A. and Mahmoud, S.R. (2017), "A four variable refined nth-order shear deformation theory for mechanical and thermal buckling analysis of functionally graded plates", *Geomech. Eng.*, In Press.

Farzam-Rad, S.A., Hassani, B. and Karamodin, A. (2017), "Isogeometric analysis of functionally graded plates using a new quasi-3D shear deformation theory based on physical neutral surface", *Compos. Part B*, **108**, 174-189.

Ferreira, A.J.M., Batra, R.C., Roque, C.M.C., Qian, L.F. and Martins, P.A.L.S. (2005), "Static analysis of functionally graded plates third-order shear deformation theory and a meshless method", *Compos. Struct.*, **69**(4), 449-457.

Ferreira, A.J.M., Batra, R.C., Roque, C.M.C., Qian, L.F. and Jorge, R.M.N. (2006), "Natural frequencies of functionally graded plates by a meshless method", *Compos. Struct.*, **75**(1-4), 593-600.

Fourn, H., Ait Atmane, H., Bourada, M., Bousahla, A.A., Tounsi, A. and Mahmoud, S.R. (2018), "A novel four variable refined plate theory for wave propagation in functionally graded material plates", *Steel Compos. Struct.*, **27**(1), 109-122.

Gasik, M. and Lilius, R. (1994), "Evaluation of properties of W-Cu functional gradient materials by micromechanical model", *Comput. Mater. Sci.*, **3**(1), 41-49.

Gasik, M.M. (1998), "Micromechanical modeling of functionally graded materials", *Comput. Mater. Sci.*, **13**(1-3), 42-55.

Golabchi, H., Kolahchi, R. and Rabani Bidgoli, M. (2018), "Vibration and instability analysis of pipes reinforced by SiO2 nanoparticles considering agglomeration effects", *Comput. Concrete*, **21**(4), 431-440.

Gupta, A. and Talha, M. (2016), "An assessment of a non-polynomial based higher order shear and normal deformation theory for vibration response of gradient plate with initial geometric imperfections", *Compos. Part B*, **107**, 141-161.

Hachemi, H., Kaci, A., Houari, M.S.A., Bourada, A., Tounsi, A. and Mahmoud, S.R. (2017), "A new simple three-unknown shear deformation theory for bending analysis of FG plates resting on elastic foundations", *Steel Compos. Struct.*, **25**(6), 717-726.

Hajmohammad, M.H., Zarei, M.S., Nouri, A. and Kolahchi, R. (2017), "Dynamic buckling of sensor/functionally graded-carbon nanotube-reinforced laminated plates/actuator based on sinusoidal-visco-piezoelasticity theories", *J. Sandw. Struct. Mater.*, In Press.

Hajmohammad, F.A. and Kolahchi, R. (2018a), "Smart control and vibration of viscoelastic actuator-multiphase nanocomposite conical shells-sensor considering hygrothermal load based on layerwise theory", *Aerosp. Sci. Technol.*, **78**, 260-270.

Hajmohammad, M.M. and Kolahchi, R. (2018b), "Seismic response of underwater concrete pipes conveying fluid covered with nano-fiber reinforced polymer layer", *Soil Dyn. Earthq. Eng.*, **110**, 18-27.

Hajmohammad, M.M., Kolahchi, R., Zarei, M.S and Maleki, M. (2018c), "Earthquake induced dynamic deflection of submerged viscoelastic cylindrical shell reinforced by agglomerated CNTs considering thermal and moisture effects", *Compos. Struct.*, **187**, 498-508.

Hamidi, A., Houari, M.S.A., Mahmoud, S.R. and Tounsi, A. (2015), "A sinusoidal plate theory with 5-unknowns and stretching effect for thermomechanical bending of functionally graded sandwich plates", *Steel Compos. Struct.*, **18**(1), 235-253.

Hazanov, S. (1998), "Hill condition and overall properties of composites", *Arch. Appl. Mech.*, **68**(6), 385-394.

Hebali, H., Tounsi, A., Houari, M.S.A., Bessaim, A. and Adda Bedia, E.A. (2014), "A new quasi-3D hyperbolic shear deformation theory for the static and free vibration analysis of functionally graded plates", *ASCE J. Eng. Mech.*, **140**(2), 374-383.

Hashin, Z. and Shtrikman, S. (1963), "A variational approach to the theory of the elastic behaviour of multiphase materials", *J. Mech. Phys. Sol.*, **11**(2), 127-140.

Hill, R. (1963), "Elastic properties of reinforced solids: Some theoretical principles", *J. Mech. Phys. Sol.*, **11**(5), 357-372.

Houari, M.S.A., Tounsi, A., Bessaim, A. and Mahmoud, S.R. (2016), "A new simple three-unknown sinusoidal shear deformation theory for functionally graded plates", *Steel Compos. Struct.*, **22**(2), 257-276.

Kaci, A., Houari, M.S.A., Bousahla, A.A., Tounsi, A. and Mahmoud, S.R. (2018), "Post-buckling analysis of shear-deformable composite beams using a novel simple two-unknown beam theory", *Struct. Eng. Mech.*, **65**(5), 621-631.

Karami, B. and Janghorban, M. (2016), "Effect of magnetic field on the wave propagation in nanoplates based on strain gradient theory with one parameter and two-variable refined plate theory", *Mod. Phys. Lett. B*, **30**(36), 1650421.

Karami, B., Shahsavari, D. and Janghorban, M. (2017a), "Wave propagation analysis in functionally graded (FG) nanoplates under in-plane magnetic field based on nonlocal strain gradient theory and four variable refined plate theory", *Mech. Adv. Mater. Struct.*, In Press.

Karami, B., Janghorban, M. and Tounsi, A. (2017b), "Effects of triaxial magnetic field on the anisotropic nanoplates", *Steel Compos. Struct.*, **25**(3), 361-374.

Karami, B., Janghorban, M. and Li, L. (2018a), "On guided wave propagation in fully clamped porous functionally graded nanoplates", *Acta Astronaut.*, **143**, 380-390.

Karami, B., Shahsavari, D. and Li, L. (2018b), "Temperature-dependent flexural wave propagation in nanoplate-type porous heterogenous material subjected to in-plane magnetic field", *J. Therm. Stress.*, **41**(4), 483-499.

Karami, B., Shahsavari, D., Li, L., Karami, M. and Janghorban, M. (2018c), "Thermal buckling of embedded sandwich piezoelectric nanoplates with functionally graded core by a nonlocal second-order shear deformation theory", *Proceedings of the Institution of Mechanical Engineers*.

Karami, B., Janghorban, M. and Tounsi, A. (2018d), "Nonlocal strain gradient 3D elasticity theory for anisotropic spherical nanoparticles", *Steel Compos. Struct.*, **27**(2), 201-216.

Karami, B., Janghorban, M. and Tounsi, A. (2018e), "Variational approach for wave dispersion in anisotropic doubly-curved nanoshells based on a new nonlocal strain gradient higher order shell theory", *Thin-Wall. Struct.*, **129**, 251-264.

Kar, V.R. and Panda, S.K. (2015), "Nonlinear flexural vibration of shear deformable functionally graded spherical shell panel", *Steel Compos. Struct.*, **18**(3), 693-709.

Khetir, H., Bachir Bouiadjra, M., Houari, M.S.A., Tounsi, A. and Mahmoud, S.R. (2017), "A new nonlocal trigonometric shear deformation theory for thermal buckling analysis of embedded nanosize FG plates", *Struct. Eng. Mech.*, **64**(4), 391-402.

Klouche, F., Darcherif, L., Sekkal, M., Tounsi, A. and Mahmoud, S.R. (2017), "An original single variable shear deformation theory for buckling analysis of thick isotropic plates", *Struct. Eng. Mech.*, **63**(4), 439-446.

Kolahchi, R. and Moniri Bidgoli, A.M. (2016), "Size-dependent sinusoidal beam model for dynamic instability of single-walled carbon nanotubes", *Appl. Math. Mech.*, **37**(2), 265-274.

Kolahchi, R., Hosseini, H. and Esmailpour, M. (2016a), "Differential cubature and quadrature-Bolotin methods for dynamic stability of embedded piezoelectric nanoplates based on visco-nonlocal-piezoelasticity theories", *Compos. Struct.*, **157**, 174-186.

Kolahchi, R., Safari, M. and Esmailpour, M. (2016b), "Dynamic stability analysis of temperature-dependent functionally graded CNT-reinforced visco-plates resting on orthotropic elastomeric medium", *Compos. Struct.*, **150**, 255-265.

Kolahchi, R., Zarei, M.S., Hajmohammad, M.H. and Oskouei, A.N. (2017a), "Visco-nonlocal-refined zigzag theories for dynamic buckling of laminated nanoplates using differential cubature-Bolotin methods", *Thin-Wall. Struct.*, **113**, 162-169.

Kolahchi, R., Zarei, M.S., Hajmohammad, M.H. and Nouri, A. (2017b), "Wave propagation of embedded viscoelastic FG-CNT-reinforced sandwich plates integrated with sensor and

actuator based on refined zigzag theory", *Int. J. Mech. Sci.*, **130**, 534-545.
Kolahchi, R., Keshtegar, B. and Fakhar, M.H. (2017c), "Optimization of dynamic buckling for sandwich nanocomposite plates with sensor and actuator layer based on sinusoidal-visco-piezoelasticity theories using Grey Wolf algorithm", *J. Sandw. Struct. Mater.*, In Press.
Kolahchi, R. and Cheraghbak, A. (2017), "Agglomeration effects on the dynamic buckling of viscoelastic microplates reinforced with SWCNTs using Bolotin method", *Nonlin. Dyn.*, **90**(1), 479-492.
Kolahchi, R. (2017), "A comparative study on the bending, vibration and buckling of viscoelastic sandwich nano-plates based on different nonlocal theories using DC, HDQ and DQ methods", *Aerosp. Sci. Technol.*, **66**, 235-248.
Klusemann, B. and Svendsen, B. (2010), "Homogenization methods for multi-phase elastic composites: Comparisons and benchmarks", *Technol. Mech.*, **30**(4), 374-386.
Koizumi, M. (1993), "Concept of FGM", *Ceram. Tran.*, **34**, 3-10.
Koizumi, M. (1997), "FGM activities in Japan", *Compos. Part B*, **28**(1-2), 1-4.
Larbi Chaht, F., Kaci, A., Houari, M.S.A., Tounsi, A., Anwar Bég, O. and Mahmoud, S.R. (2015), "Bending and buckling analyses of functionally graded material (FGM) size-dependent nanoscale beams including the thickness stretching effect", *Steel Compos. Struct.*, **18**(2), 425-442.
Liu, B., Ferreira, A.J.M., Xing, Y.F. and Neves, A.M.A. (2016), "Analysis of functionally graded sandwich and laminated shells using a layerwise theory and a differential quadrature finite element method", *Compos. Struct.*, **136**, 546-553.
Madani, H., Hosseini, H. and Shokravi, M. (2016), "Differential cubature method for vibration analysis of embedded FG-CNT-reinforced piezoelectric cylindrical shells subjected to uniform and non-uniform temperature distributions", *Steel Compos. Struct.*, **22**(4), 889-913.
Mahi, A., Adda Bedia, E.A. and Tounsi, A. (2015), "A new hyperbolic shear deformation theory for bending and free vibration analysis of isotropic, functionally graded, sandwich and laminated composite plates", *Appl. Math. Model.*, **39**(9), 2489-2508.
Meksi, R, Benyoucef, S., Mahmoudi, A., Tounsi, A., Adda Bedia, E.A. and Mahmoud, S.R. (2018), "An analytical solution for bending, buckling and vibration responses of FGM sandwich plates", *J. Sandw. Struct. Mater.*, 1099636217698443.
Menasria, A., Bouhadra, A., Tounsi, A., Bousahla, A.A. and Mahmoud, S.R. (2017), "A new and simple HSDT for thermal stability analysis of FG sandwich plates", *Steel Compos. Struct.*, **25**(2), 157-175.
Meradjah, M., Kaci, A., Houari, M.S.A., Tounsi, A. and Mahmoud, S.R. (2015), "A new higher order shear and normal deformation theory for functionally graded beams", *Steel Compos. Struct.*, **18**(3), 793-809.
Mokhtar, Y., Heireche, H., Bousahla, A.A., Houari, M.S.A., Tounsi, A. and Mahmoud, S.R. (2018), "A novel shear deformation theory for buckling analysis of single layer graphene sheet based on nonlocal elasticity theory", *Smart Struct. Syst.*, **21**(4), 397-405.
Mouffoki, A., Adda Bedia, E.A., Houari, M.S.A., Tounsi, A. and Mahmoud, S.R. (2017), "Vibration analysis of nonlocal advanced nanobeams in hygro-thermal environment using a new two-unknown trigonometric shear deformation beam theory", *Smart Struct. Syst.*, **20**(3), 369-383.
Paulino, G.H., Jin, Z.H. and Dodds Jr, R.H. (2003), *Comprehensive Structural Integrity, Vol.2: Fundamental Theories and Mechanisms of Failure, Chapter 13: Failure of Functionally Graded Materials*, Elsevier Science.
Rahman, S. and Chakraborty, A. (2007), "A stochastic micromechanical model for elastic properties of functionally graded materials", *Mech. Mater.*, **39**(6), 548-563.
Reiter, T. and Dvorak, G.J. (1997), "Micromechanical models for graded composite materials", *J. Mech. Phys. Sol.*, **45**(8), 1281-1302.
Reiter, T. and Dvorak, G.J. (1998), "Micromechanical models for graded composite materials: II. Thermomechanical loading", *J. Mech. Phys. Sol.*, **46**(9), 1655-1673.
Reuss, A. (1929), "Berechnung der fliessgrenze von mischkristallen auf grund der plastizitätsbedingung für einkristalle", *Z Angew. Math. Mech.*, **9**(1), 49-58.
Schmauder, S. and Weber, U. (2001), "Modelling of functionally graded materials by numerical homogenization", *Arch. Appl. Mech.*, **71**(2-3), 183-193.
Sekkal, M., Fahsi, B., Tounsi, A. and Mahmoud, S.R. (2017a), "A novel and simple higher order shear deformation theory for stability and vibration of functionally graded sandwich plate", *Steel Compos. Struct.*, **25**(4), 389-401.
Sekkal, M., Fahsi, B., Tounsi, A. and Mahmoud, S.R. (2017b), "A new quasi-3D HSDT for buckling and vibration of FG plate", *Struct. Eng. Mech.*, **64**(6), 737-749.
Shabana, Y.M. and Nota, N. (2008), "Numerical evaluation of the thermomechanical effective properties of a functionally graded material using the homogenization method", *Int. J. Sol. Struct.*, **45**(11-12), 3494-3506.
Shahsavari, D. and Janghorban, M. (2017), "Bending and shearing responses for dynamic analysis of single-layer graphene sheets under moving load", *J. Braz. Soc. Mech. Sci. Eng.*, **39**(10), 3849-3861.
Shahsavari, D., Shahsavarib, M., Li, L. and Karami, B. (2018), "A novel quasi-3D hyperbolic theory for free vibration of FG plates with porosities resting on Winkler/Pasternak/Kerr foundation", *Aerosp. Sci. Technol.*, **72**, 134-149.
Shahsavari, D., Karami, B. and Mansouri, S. (2018), "Shear buckling of single layer graphene sheets in hygrothermal environment resting on elastic foundation based on different nonlocal strain gradient theories", *Eur. J. Mech.-A/Sol.*, **67**, 200-214.
Shen, H.S. and Wang, Z.X. (2012), "Assessment of Voigt and Mori-Tanaka models for vibration analysis of functionally graded plates", *Compos. Struct.*, **94**(7), 2197-2208.
Sobhy, M. (2013)," Buckling and free vibration of exponentially graded sandwich plates resting on elastic foundations under various boundary conditions", *Compos. Struct.*, **99**, 76-87.
Shokravi, M. (2017a), "Vibration analysis of silica nanoparticles-reinforced concrete beams considering agglomeration effects", *Comput. Concrete*, **19**(3), 333-338.
Shokravi, M. (2017b), "Buckling analysis of embedded laminated plates with agglomerated CNT-reinforced composite layers using FSDT and DQM", *Geomech. Eng.*, **12**(2), 327-346.
Shokravi, M. (2017c), "Dynamic pull-in and pull-out analysis of viscoelastic nanoplates under electrostatic and Casimir forces via sinusoidal shear deformation theory", *Microelectr. Reliab.*, **71**, 17-28.
Shokravi, M. (2017d), "Buckling of sandwich plates with FG-CNT-reinforced layers resting on orthotropic elastic medium using Reddy plate theory", *Steel Compos. Struct.*, **23**(6), 623-631.
Thai, C.H., Zenkour, A.M., Abdel Wahab, M. and Nguyen-Xuan, H. (2016), "A simple four-unknown shear and normal deformations theory for functionally graded isotropic and sandwich plates based on isogeometric analysis", *Compos. Struct.*, **139**, 77-95.
Tossapanon, P. and Wattanasakulpong, N. (2016), "Stability and free vibration of functionally graded sandwich beams resting on two-parameter elastic foundation", *Compos. Struct.*, **142**, 215-225.

Tounsi, A., Houari, M.S.A., Benyoucef, S. and Adda Bedia, E.A. (2013), "A refined trigonometric shear deformation theory for thermoelastic bending of functionally graded sandwich plates", *Aerosp. Sci. Technol.*, **24**(1), 209-220.

Touratier, M. (1991), "An efficient standard plate theory", *Eng. Sci.*, **29**(8), 901-916.

Vel, S.S. and Batra, R.C. (2004), "Three-dimensional exact solution for the vibration of functionally graded rectangular plates", *J. Sound Vibr.*, **272**(3-5), 703-730.

Voigt,W. (1889), "Über die beziehung zwischen den beiden elastizitätskonstanten isotroper körper", *Wied. Ann. Phys.*, **38**(2), 573-587.

Yamanouchi, M., Koizumi, M., Hirai, T. and Shiota, I. (1990), *Proceedings of the 1st International Symposium Functionally Gradient Material*, Japan.

Yazid, M., Heireche, H., Tounsi, A., Bousahla, A.A. and Houari, M.S.A. (2018), "A novel nonlocal refined plate theory for stability response of orthotropic single-layer graphene sheet resting on elastic medium", *Smart Struct. Syst.*, **21**(1), 15-25.

Yin, H.M., Sun, L.Z. and Paulinho, G.H. (2004), "Micromechanics-based elastic model for functionally graded materials with particle interactions", *Acta Mater.*, **52**(12), 3535-3543.

Yin, H.M., Paulinho, G.H., Buttlar, W.G. and Sun, L.Z. (2007), "Micromechanics-based thermoelastic model for functionally graded particulate materials with particle interactions", *J. Mech. Phys. Sol.*, **55**(1), 132-160.

Youcef, D.O., Kaci, A., Benzair, A., Bousahla, A.A. and Tounsi, A. (2018), "Dynamic analysis of nanoscale beams including surface stress effects", *Smart Struct. Syst.*, **21**(1), 65-74.

Younsi, A., Tounsi, A, Zaoui, F.Z., Bousahla, A.A. and Mahmoud, S.R. (2018), "Novel quasi-3D and 2D shear deformation theories for bending and free vibration analysis of FGM plates", *Geomech. Eng.*, **14**(6), 519-532.

Zamanian, M., Kolahchi, R. and Bidgoli, M.R. (2017), "Agglomeration effects on the buckling behaviour of embedded concrete columns reinforced with SiO_2 nano-particles", *Wind Struct.*, **24**(1), 43-57.

Zarei, M.S., Kolahchi, R., Hajmohammad, M.H. and Maleki, M. (2017), "Seismic response of underwater fluid-conveying concrete pipes reinforced with SiO2 nanoparticles and fiber reinforced polymer (FRP) layer", *Soil Dyn. Earthq. Eng.*, **103**, 76-85.

Zemri, A., Houari, M.S.A., Bousahla, A.A. and Tounsi, A. (2015), "A mechanical response of functionally graded nanoscale beam: an assessment of a refined nonlocal shear deformation theory beam theory", *Struct. Eng. Mech.*, **54**(4), 693-710.

Zidi, M., Tounsi, A., Houari, M.S.A., Adda Bedia, E.A. and Anwar Bég, O. (2014), "Bending analysis of FGM plates under hygro-thermo-mechanical loading using a four variable refined plate theory", *Aerosp. Sci. Technol.*, **34**, 24-34.

Zidi, M., Houari, M.S.A., Tounsi, A., Bessaim, A. and Mahmoud, S.R. (2017), "A novel simple two-unknown hyperbolic shear deformation theory for functionally graded beams", *Struct. Eng. Mech.*, **64**(2), 145-153.

Zine, A., Tounsi, A., Draiche, K., Sekkal, M. and Mahmoud, S.R. (2018), "A novel higher-order shear deformation theory for bending and free vibration analysis of isotropic and multilayered plates and shells", *Steel Compos. Struct.*, **26**(2), 125-137.

Zuiker, J.R. (1995), "Functionally graded materials: Choice of micromechanics model and limitations in property variation", *Compos. Eng.*, **5**(7), 807-819.

CC